Tunnelling and Underground Space Technology 141 (2023) 105316

Contents lists available at ScienceDirect

Tunnelling and Underground Space Technology

journal homepage: www.elsevier.com/locate/tust

Analytical prediction for ground movements due to deep excavations in soils

Chen Zheng [a], Andrea Franza [b,*], Rafael Jimenez [a]

[a] ETSI Caminos, Canales y Puertos, Universidad Politécnica de Madrid, Madrid, Spain
[b] Department of Civil and Architectural Engineering, Aarhus University, Aarhus, Denmark

ARTICLE INFO

Keywords:
Deep excavation
Soil deformation
Settlement
Horizontal movements
Analytical solution
Ground loss

ABSTRACT

This paper presents an analytical method to estimate surface and subsurface soil movements induced by deep excavations in the vertical and horizontal directions. Elastic and elastoplastic closed-form solutions for ground losses in the half-space are adopted, using the superposition method, to consider convergence and ovalization processes that occur within the soil mass due to displacements of the retaining wall; inputs include the shape and magnitude of the wall displacement profile to be selected based on design charts, monitoring data, or allowable level of resulting ground deformations. A parametric analysis illustrates (i) the effects on greenfield soil movements of the retaining wall's deformation modes (cantilever, parabolic, composite, or kick-in), (ii) the influence of its displacement level, and (iii) the influence of aspects such as the soil's ovalization and volumetric behaviour. Predictions of the proposed method are compared with empirical criteria, field data, and centrifuge results from the literature compiled for braced excavations in clays and sands. This comparison shows that the analytical approach provides reasonable predictions of excavation-induced soil deformations both at surface and subsurface levels, except for high normalized wall deflections when the analytical ground displacement field is wider and its maximum movements underestimate measured values. Finally, from the back-analyses of real data, a design guideline is suggested to select the relative ovalization depending on ground conditions and wall deflection mode.

1. Introduction

New construction activities often require deep excavations in congested urban environments. To minimize their impact on adjacent buildings or other infrastructure, deep retaining walls with an adequate construction sequence should be carefully designed to minimize ground movements (Boone et al., 1999; Son and Cording, 2007; Elshafie et al., 2013; Korff et al., 2016; Soomro et al., 2019); whereas, to prevent over-engineering and excessive costs, the deep excavation design should still allow for some wall displacements and ground deformations during excavation. Inevitably, wall displacements become a source of ground losses within the surrounding soil, that moves towards the excavation.

Soil movements induced by such deep excavations are the result of complex phenomena that depend on many factors such as soil conditions, type of retaining wall and construction sequence. For instance, as shown in Fig. 1, different ground conditions or different construction methods may lead to concave- or spandrel-type surface settlement profiles (Clough and O'Rourke, 1990; Hsieh and Ou, 1998). Advanced numerical modelling is an effective tool for design of deep excavations, as it allows one to consider complex ground constitutive behaviour or complex construction sequences (Finno and Harahap, 1991; Kung et al., 2007b; Yoo and Lee, 2008; Khoiri and Ou, 2013; Dong et al., 2016; Zheng et al., 2018; Soomro et al., 2019), and to couple it with the inverse method for model calibration (Finno and Calvello, 2005; Kim and Finno, 2019). However, the calibration of advanced numerical models is complex and time-consuming, and simple analytical methods can be useful to estimate the soil movements and deformations, for instance, (i) at preliminary design stages, when ground information is limited and budget and time constraints may also exist, or (ii) during the excavation phases.

In addition to research outputs from field monitoring (Burland and Hancock, 1977; Finno et al., 1989; Tan and Wei, 2012; Liu et al., 2019; Hsiung, 2020) and from experimental investigations (Ong et al., 2006; Lam et al., 2014; Ng et al., 2017), engineers often rely on empirical approaches for the preliminary estimate of excavation-induced ground movements at the surface (Peck, 1969; Clough and O'Rourke, 1990; Ou et al., 1993; Hsieh and Ou, 1998; Kung et al., 2007a; Ou and Hsieh, 2011). However, empirical expressions for subsurface movements are limited to specific site conditions (Mu and Huang, 2016). Therefore, analytical (closed-form) methods to estimate surface and subsurface movements are needed, so that researchers and practitioners can develop fast, yet accurate, estimates of excavation-induced

* Corresponding author.
E-mail address: anfr@cae.au.dk (A. Franza).

https://doi.org/10.1016/j.tust.2023.105316
Received 11 November 2020; Received in revised form 23 December 2022; Accepted 6 July 2023
Available online 3 August 2023

Notation

H_c	Cavity depth
H	Excavation depth
H_w	Wall length
R	Radius of the cavity
u_x	Horizontal subsurface movement
u_x^{cav}	Horizontal movement due to a cavity volume loss
$u_{x,0}$	Horizontal surface movement
$u_{x,0}^{max}$	Maximum horizontal surface movement
u_z	Vertical subsurface movement
u_z^{cav}	Vertical movement due to a cavity volume loss
$u_{z,0}$	Vertical surface movement
$u_{z,0}^{max}$	Maximum vertical surface movement
u_Δ	Ovalization displacement
u_ε	Convergence displacement
$V_{l,s}$	Soil volume loss
$V_{l,w}$	Volume loss due to the horizontal wall deflection
x	Horizontal spatial coordinate
z	Vertical spatial coordinate
α	Ground volumetric parameter
β	Wall displacement level
Δ	Ovalization parameter
ΔH	Length of the wall segment
δ	Horizontal wall deflection
$\bar{\delta}$	Average value of horizontal wall deflection
δ^{max}	Maximum wall deflection
ε	Contraction parameter
ρ	Relative ovalization
M1	Cantilever-type of wall deflection
M2	Parabola-type of wall deflection
M3	Composite-type of wall deflection
M4	Kick-in-type of wall deflection

ground deformations which may affect other buildings or infrastructure. For instance, such analytical solutions of greenfield movements associated with deep excavations are required as an input to simplified soil–structure interaction models to assess the effects due to deep excavations, similar to the approach employed to assess soil–structure interaction effects due to tunnelling (Verruijt and Booker, 1996; Loganathan and Poulos, 1998).

The Mobilizable Strength Design (MSD) method based on the theory of plasticity has been implemented by Osman and Bolton (2004, 2006) to predict wall deflections and ground surface settlements due to undrained excavations of deep walls. Lam and Bolton (2011) extended the MSD method to analyse wide excavations in relatively shallow soft clay strata or narrow excavations in relatively deep soft strata. Note that available applications of MSD are limited to the prediction of surface settlements. Dan and Sahu (2018) proposed a minimum potential energy approach to estimate ground movements and wall deflections due to deep excavations. However, ground movement (e.g., surface settlement) patterns need to be assumed a priori in this approach, hence affecting the rigorousness of this method. A simplified analytical method (Cheng et al., 2020) has been proposed to estimate (elastic) excavation-induced soil movements under plane strain. This proposed solution can consider arbitrary deflections of the supporting structure. However, this study focused on lateral ground movements and it did not report settlements, thus limiting its applicability in practice. Elastic methods that superimpose sources of ground loss are also available (Sagaseta, 1987; Zhang et al., 2011); however, systematic validation of their performance against the field and experimental data is missing from the literature. Generally, all the above methods related the ground movement to the supporting structure's deformation, but the effect of uneven stress relief on the behaviour of soil (resulting in the ground loss ovalization) is neglected in their solutions. Also, a reliable method to predict horizontal surface and subsurface soil movements is still lacking. The analytical method in this paper addresses these shortcomings.

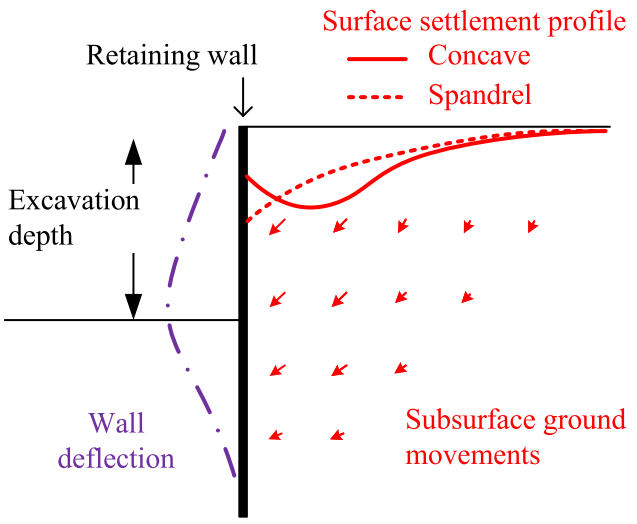

Fig. 1. Excavation-induced wall deflection and ground movements at the retained side.

This paper provides an effort in this direction and employs analytical closed-form solutions, based on the superposition of ground losses in the half-space, to estimate ground movements induced by deep excavations conducted in clays or sands. Firstly, the main dimensionless factors affecting the excavation-induced soil deformation mechanisms are analysed. Then, to ensure practical relevance, an extensive dataset of empirical envelopes and well-documented case histories and experimental data is used to evaluate the performance of the proposed formulas, which allow one to rationally account for the wall deformation mode and for fundamental aspects of ground behaviour.

2. Analytical method

In this paper, excavation-induced surface ground movements are denoted as $u_{z,0}$ and $u_{x,0}$, respectively; while subsurface displacements are denoted as u_z and u_x. To evaluate the excavation-induced movements of the ground, the displacement field due to a distributed ground loss associated with the excavation can be computed by integrating point ground losses occurring along the retaining wall.

To that end, displacements due to a point sink should be defined first. The vertical and horizontal movements due to a near-surface circular cavity in an isotropic, homogeneous, and incompressible medium (i.e., for undrained soil conditions) were computed by Sagaseta (1987) using the superposition of singularities technique. Verruijt and Booker (1996) extended this solution to consider the effects of two mechanisms: (i) the decrease in spherical stresses associated with the ground loss (the so-called convergence mechanism); and (ii) the relief of deviatoric stresses that occurs at the cavity (leading to the ground ovalization mechanism). Fig. 2a shows the effects of such mechanisms on the cavity movements associated with an infinitely deep sink, when the surface influence is neglected. The convergence parameter and the ovalization parameter are hence defined as $\varepsilon = u_\varepsilon/R$ and $\Delta = u_\Delta/R$, respectively, where R is the original cavity radius, u_ε is the uniform convergence

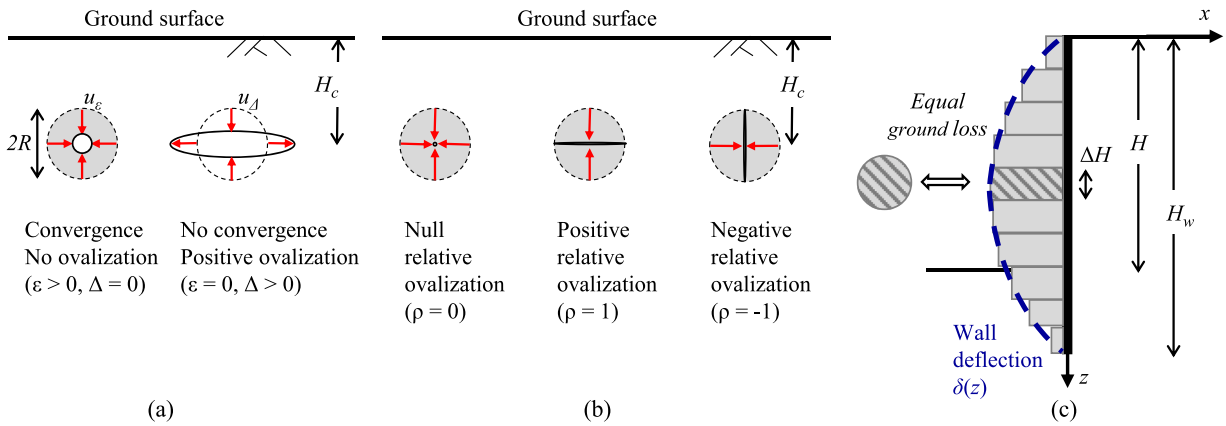

Fig. 2. Illustration of (a) cavity deformations associated with convergence or ovalization mechanisms, for a deep sink ($H_c \to \infty$); (b) ground losses for varying relative ovalization; (c) basis of the prediction method: distributed circular ground losses (equal in volume to original rectangular volume losses) imposed along the retaining wall to model the wall deflection.

displacement and u_Δ is the maximum ovalization displacement; as shown in Fig. 2a, ε is considered positive for a ground loss, and Δ is considered positive for outwards horizontal movements (elongations) at the cavity springline.

In this work, the ovalization level is described by the relative ovalization, $\rho = \Delta/\varepsilon$, whose effects on deep cavity distortions are displayed in Fig. 2b for cases with: null ovalization ($\rho = 0$); positive ovalization with minimal horizontal displacement at the springline ($\rho = 1$); and negative ovalization with minimal vertical displacement at the cavity crown and bottom ($\rho = -1$). Considering the relationship between relative ovalization and stresses for deep cavities, the relative ovalization ρ tends towards negative values for cases with a high coefficient of earth pressure at rest (Verruijt and Booker, 1998). Also, González and Sagaseta (2001) pointed out that ρ can take positive and negative values depending on pressure distributions and uneven stress relief in tunnelling. Finally, to account for the effect of soil volumetric deformations, the ground volumetric parameter α was introduced by González and Sagaseta (2001) to account for the observation that displacements due to the ground loss in the plastic zone that forms around a tunnel attenuates as a power function of the distance from the cavity.

From these works, and considering the soil ovalization and volumetric deformations, González and Sagaseta (2001) indicated that the vertical (u_z^{cav}) and horizontal (u_x^{cav}) soil movements due to a cavity ground loss are:

$$\frac{u_x^{cav}}{2\varepsilon R\left(\frac{R}{H_c}\right)^{2\alpha-1}} = -\frac{x'}{2r_1'^{2\alpha}}\left(1-\rho\frac{x'^2-z_1'^2}{r_1'^2}\right) - \frac{x'}{2r_2'^{2\alpha}}\left(1-\rho\frac{x'^2-z_2'^2}{r_2'^2}\right) + \frac{4x'z'}{2r_2'^{2\alpha}}\left(\frac{z_2'}{r_2'^2}-\rho\frac{x'^2-3z_2'^2}{r_2'^4}\right) \quad (1)$$

$$\frac{u_z^{cav}}{2\varepsilon R\left(\frac{R}{H_c}\right)^{2\alpha-1}} = -\frac{z_1'}{2r_1'^{2\alpha}}\left(1-\rho\frac{x'^2-z_1'^2}{r_1'^2}\right) + \frac{z_2'}{2r_2'^{2\alpha}}\left(1+\rho\frac{x'^2-z_2'^2}{r_2'^2}\right) - \frac{1}{2r_2'^{2\alpha}}\left(2\left(z'+\rho\right)\frac{x'^2-z_2'^2}{r_2'^2}+4\rho z'z_2'\frac{3x'^2-z_2'^2}{r_2'^4}\right) \quad (2)$$

where x and z are the horizontal and vertical spatial coordinates (considering the origin of coordinates at the retaining wall top), H_c is the depth to the centre of the cavity, R is the radius of the cavity, $z_1 = z - H_c, z_2 = z + H_c, r_1 = \sqrt{x^2+(z-H_c)^2}, r_2 = \sqrt{x^2+(z+H_c)^2}$, and where the prime indicates that the variable is scaled by H_c (e.g., $z_1' = z_1/H_c$). See Fig. 2.

Next, the displacement field due to a deep excavation is obtained by integrating (superposing) the solutions above, as shown in Eq. (3). That is, the displacement field due to a distributed ground loss can be computed by integration (superposition) of point ground losses, as firstly suggested by Sagaseta (1987) for a pile removal analysis. Adopting a similar logic, Xu and Poulos (2000) and Zhang et al. (2011) suggested that deflections of a retaining wall δ (i.e., its horizontal displacement profile against depth z; see Fig. 2c) are associated with a distributed ground loss, given by the superposition of cavity displacements predicted by Sagaseta (1987). In particular, such excavation-induced displacements are obtained by the superposition of displacements (u_x^{cav} and u_z^{cav}) produced by n point sinks that produce an equivalent ground loss, and that are distributed along the retaining wall, as shown in Fig. 2(c). And, by dividing the wall height H_w into n segments of depth ΔH ($\Delta H = 0.01$ m was used in this work), the ground loss of each circular cavity $2\varepsilon\pi R^2$ is made equal to the rectangular volume loss $m\delta\Delta H$, where the factor $m = 2$ is needed to consider that the cavity solution applies to the soil quarter supported by the retaining wall, rather than to the full half-space. We get:

$$u_x = \sum_{i=1}^{n} u_{x,i}^{cav}, \qquad u_z = \sum_{i=1}^{n} u_{z,i}^{cav} \quad (3)$$

To improve previous methods for elastic ground displacement prediction by considering the influence of ground ovalization (ρ) and volumetric behaviour (α), this paper proposes that the point sink induced movements ($u_{x,i}^{cav}$ and $u_{z,i}^{cav}$) to be used in Eq. (3) should be computed using Eqs. (1) and (2), rather than using the model of Sagaseta (1987) of uniform convergence and incompressible soil. As the results will illustrate, the physical significance of ovalization is relevant, due to the initially anisotropic stress field that exists in most soil formations, and to the excavation-induced horizontal stress relief that is expected to occur in typical deep walls; similarly, soil volumetric strains could also be relevant, especially when associated with positive/negative dilatancy of the ground in drained conditions ($\alpha = 1$ should be used for undrained conditions).

As shown above, the wall horizontal displacement profile, δ (considering both its shape and magnitude), becomes a crucial input of this analytical prediction method, and it is to a large extent determined by aspects such as soil conditions, excavation and wall geometry, and the support system adopted (e.g., unsupported wall, single or multiple props for braced excavations, etc.). Before the construction, the expected wall deflection distribution δ can be inferred from the previous field or laboratory experience for similar soil conditions and support systems. For instance, design charts describing the expected ratio between maximum wall deflections and excavation depths are available (Leung and Ng, 2007; Tan and Wei, 2012; Gaba et al., 2017; Cheng et al., 2021); alternatively, the wall deflection distribution can be estimated from the beam on elastic foundation method (Zhang et al.,

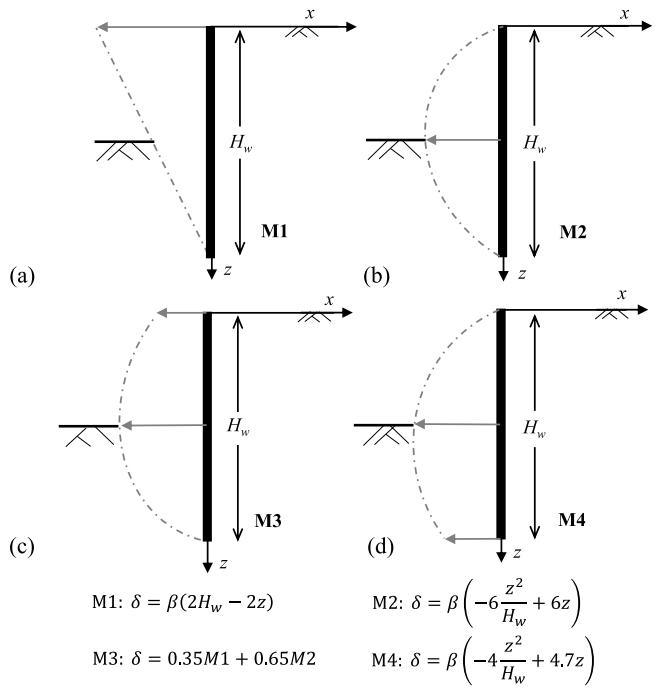

Fig. 3. Considered profiles of wall deflection δ: (a) cantilever-type M1, (b) parabola-type M2, (c) composite-type M3, (d) kick-in-type M4.

2011; Guo et al., 2019). Alternatively, the proposed solution may also be used during the excavation to estimate ground movements, from wall deflections (used as input) that can be easily monitored.

Considering field evidence (see e.g., Goldberg et al., 1976; Ng, 1998; Liu et al., 2005; Ng et al., 2012; Khoiri and Ou, 2013), the four fundamental wall deflection modes (M1 to M4) illustrated by Fig. 3 are considered in this paper namely: cantilever-type (M1), parabola-type (M2), composite-type (M3), and kick-in-type (M4). Their equations are listed in Fig. 3. Although there may be uncertainties related to the expected wall deflection during preliminary design stages, the simplicity of the analytical method allows for either probabilistic or upper estimates of the distribution of excavation-induced ground movements (in both vertical and horizontal directions) to be easily computed, which could then be used to estimate the sensitivity of nearby foundations or infrastructure to such expected/allowable ground deformations or differential movements.

Furthermore, the wall displacement level $\beta = \bar{\delta}/H_w$ – defined as the ratio between average wall deflection and wall height – is employed to characterize the (relative) magnitude of wall deflections. Alternatively, β can also be expressed as $\beta = V_{l,w}/H_w^2$, where $V_{l,w}$ is the volume loss due to the horizontal wall deflection; therefore, the wall displacement level also normalises the wall volume loss $V_{l,w}$ (volume per running meter) given by a distributed ground loss.

Based on the discussion above, it can be observed that the proposed analytical solution is controlled by four aspects or parameters: the wall displacement level (β) which acts as a scaling factor, since displacements increase linearly with it; the wall displacement mode (M1 to M4); the ground ovalization parameter (ρ); and the ground volumetric parameter (α). Their relative relevance is discussed in the following section. Note that, for simplicity, horizontal displacements are considered positive when associated with horizontal movements towards the excavation, and that vertical displacements are considered positive when associated with settlement (downwards).

3. Parametric study of the ground and wall input

Next, a sensitivity analysis is conducted to investigate the effects, on the ground movements, of the wall deflection mode (M1 to M4) and of given ground ovalization (ρ) and ground volumetric (α) parameters. The study is carried out for a wall depth of $H_w = 15$ m and for an average displacement of $\bar{\delta} = 15$ mm, hence leading to a value of $\beta = 0.1\%$ which is commonly achieved in the field (as discussed later in the text). Fig. 4 illustrates how surface movements are affected by the relative ground ovalization, the volumetric (dilative or contractive) soil behaviour, and the wall deformation mode; whereas Figs. 5 and 6 plot ground movements along two vertical sections at a horizontal distance of $x = 2$ m ($= 13\%H_w$) and $x = 15$ m ($= 100\%H_w$) from the wall, which are named 'close' and 'far' sections, respectively. These figures report results for M1, M2, and M3, while data for M4 are provided in supplemental data. Results are plotted in dimensionless terms, and they are discussed in the subsections below.

3.1. Soil ovalization behaviour

The deep excavation will inevitably alter the in-situ stresses within the ground, and the associated ground ovalization could hence influence the resulting displacement field. Therefore, the effects of ρ on the ground movement distributions are investigated for limit values of negative and positive ovalization, given by $\rho = -1$ and $\rho = 1$ (i.e., for vertical and horizontal ovalization), as well as for cases with no ovalization, $\rho = 0$. See Fig. 2b.

Fig. 4a illustrates the influence of the relative ovalization for a wall deforming with a parabolic deflection mode (M2): widely different surface settlement profiles occur for different ground ovalization values. Note, for instance, that the spandrel-type settlement profile occurs for $\rho = 1$ or $\rho = 0$ and that the concave-type occurs for $\rho = -1$. The maximum surface settlement is also affected by ovalization, with positive ovalization ($\rho = 1$) producing settlements larger than 0.3% H_w, and with negative ovalization ($\rho = -1$) producing only about 20% of that value. Surface settlements extend away from the wall within an influence distance of at least twice the wall length in all cases. Fig. 4b shows the horizontal surface movements for these cases. As expected (results are for parabolic mode M2, with zero horizontal surface movements) the maximum horizontal movements occur slightly away from the wall for all ovalization cases; also note that the negative ovalization case ($\rho = -1$) produces larger horizontal movements than the other two ovalization cases ($\rho = 0$ and $\rho = 1$), and that such larger movements also extend further away from the wall.

Next, subsurface movements are discussed. Figs. 5a and 6a show that ovalization significantly changes the shape of the subsurface settlements at both the 'close' and 'far' vertical sections. Results 'close' to the wall (see Fig. 5a) indicate a sharp decrease of subsurface settlements with depth for positive and null ovalization ($\rho = 1$; $\rho = 0$), which could even lead to upwards soil movements at the wall tip ($z = H_w$); while nearly uniform settlements with depth are obtained when the ovalization is negative ($\rho = -1$). Ovalization seems to produce the opposite trend at the 'far' section (see Fig. 6a), with settlements that linearly decrease (slightly) with depth for negative ovalization, and with a quasi-constant settlement profile obtained for a positive ovalization; note, however, that settlements at the 'far' section are much smaller than those obtained 'close' to the wall. In any case, these results suggest that the commonly-employed assumption of linearly decreasing settlements with depth, adopted in excavation-pile-soil interaction analyses (Korff et al., 2016; Franza et al., 2021), could not always be fully representative for pile foundations located 'close' to the wall.

Finally, Figs. 5b and 6b indicate that a negative ground ovalization could increase the magnitude of the horizontal displacements, particularly for sections 'close' to the wall. Note also that the horizontal movement profile closely follows the M2-mode wall deflection shape, and that the horizontal movement profiles attenuate with their offset distance from the wall, transforming themselves (for the 'far' section) into shapes characterized by a linear decrease with depth.

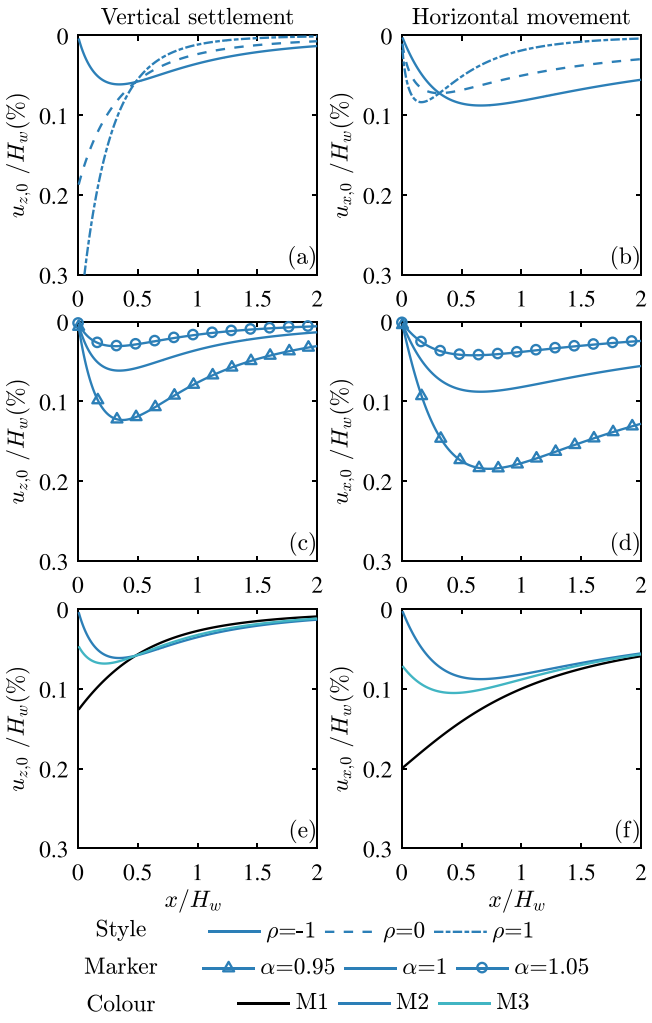

Fig. 4. Surface displacements in the vertical (left) and horizontal (right) directions, for a parabolic wall deflection of M2 mode and for $\beta = 0.1\%$: (a)–(b) influence of the ovalization in incompressible soil and (c)–(d) impact of the volumetric strain for negative ovalization ($\rho = -1$); (e)–(f) effect of the wall deflection modes M1, M2, and M3 for incompressible soil with negative ovalization ($\rho = -1$).

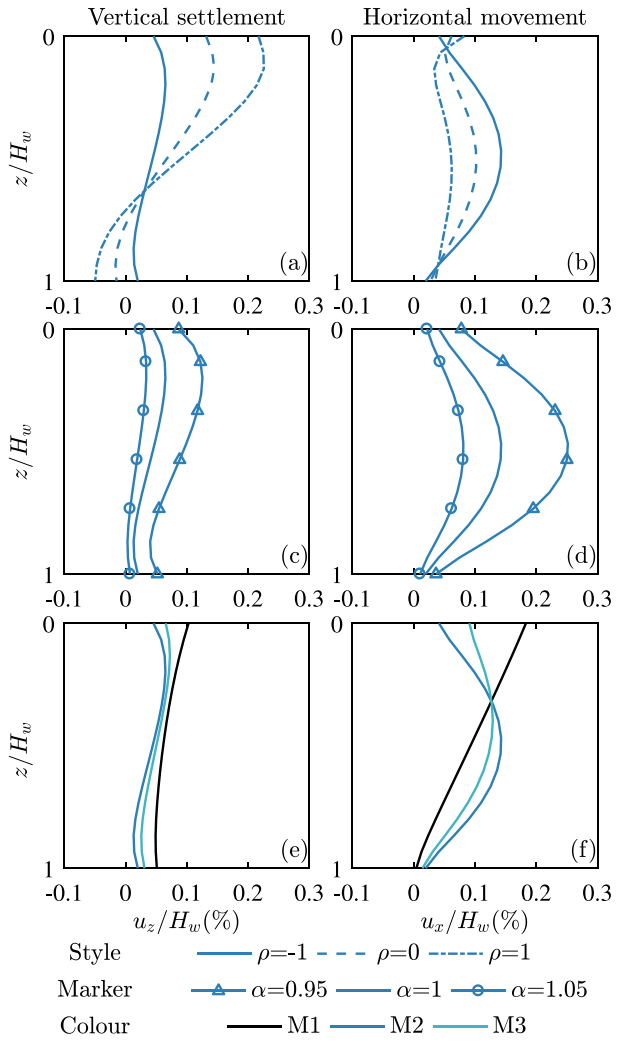

Fig. 5. Vertical (left) and horizontal (right) subsurface movements at the vertical section 'close' to the wall ($x/H_W = 13\%$).

3.2. Soil volumetric behaviour

Next, we investigate the impact of the soil volumetric behaviour (and of its coupling with the other input parameters) on the computed soil movements. To that end, the average volumetric strain parameter is selected to represent dilative ($\alpha > 1$, with $\alpha = 1.05$ being used), contractive ($\alpha < 1$, with $\alpha = 0.95$) or incompressible ($\alpha = 1$) behaviour of the ground.

Fig. 4c shows that, for all such α values considered, a concave-type surface settlement trough is obtained for a negative ovalization ($\rho = -1$). When the soil is contractive ($\alpha < 1$), surface settlements are larger and extend further away from the wall, producing a wider influence zone, although the location of the point with a maximum settlement is almost unaffected by α. In contrast, volumetric dilations decrease the magnitude of the ground settlement trough.

A similar influence of α occurs when the horizontal surface (see Fig. 4d) or subsurface movements (Figs. 5c–d and 6c–d) are considered. Therefore, it is concluded that, in the proposed solution, the volumetric parameter α impacts displacement magnitude, but that it has a limited effect on the type (or shape) of the ground displacement distribution.

3.3. Wall deflection shape

The effect of the shape of the wall displacement profile is addressed considering the four fundamental modes (M1 to M4) for a retaining wall excavated in an incompressible soil (i.e., undrained conditions, or $\alpha = 1$) with negative ovalization ($\rho = -1$), as shown in subplots e and f of Figs. 4–6. Results show that the wall deflection mode influences the distribution of displacements at the surface (see Fig. 4e and f): similar concave-type settlements profiles are observed for the parabolic (M2) and kick-in (M4) modes; a spandrel-type surface settlement profile occurs for the cantilever mode (M1); and an intermediate shape is obtained for the composite mode (M3). As discussed above for cases with different ovalization values, spandrel-type settlements tend to induce larger surface settlements and larger horizontal displacements, particularly 'closer' to the wall.

Importantly, for all deflection modes, the comparison between Fig. 4e and f indicates that the shapes of $u_{x,0}$ (horizontal) and $u_{z,0}$ (vertical) displacement distributions at the surface are similar (i.e., shapes of $u_{x,0}$ and $u_{z,0}$ are similar for a given mode), with only a different displacement magnitude (i.e., a different scale) that makes surface horizontal displacements to be significantly larger than vertical displacements: for instance, $u_{x,0}^{max} \approx 1.65\, u_{z,0}^{max}$, under M1. Thus, engineers should be aware that there may be conditions (seldom encountered) in

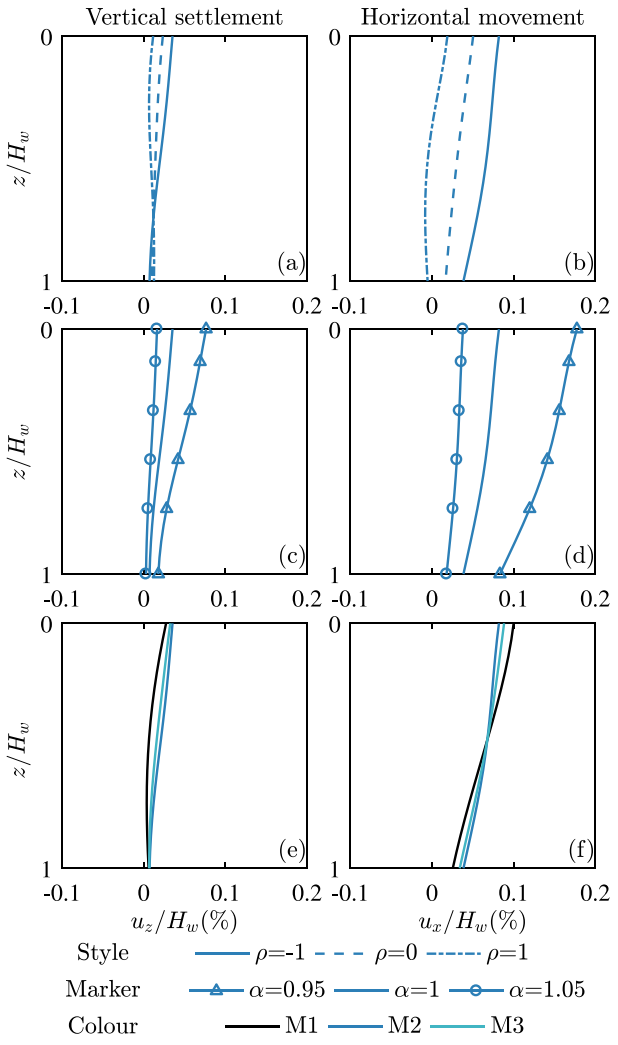

Fig. 6. Vertical (left) and horizontal (right) subsurface movements at the vertical section 'far' from the wall ($x/H_W = 100\%$).

which horizontal movements are as large as settlements, as confirmed by a few history cases considered in this paper.

Contrarily, the shape of the subsurface displacement profiles (u_x and u_z) is not comparable along the vertical sections considered. At the 'close' section, results in Fig. 5e show that the maximum subsurface settlement u_z^{max} occurs at a depth slightly below the surface for the parabolic (M2), composite (M3) and kick-in (M4) deflection modes, with vertical displacements decreasing to about zero at the wall tip ($z = H_w$). On the other hand, the maximum vertical displacement for the cantilever (M1) deflection mode occurs at the surface ($u_z^{max} \approx u_{z,0}^{max}$), and there is a (nearly) linear reduction of settlements from the surface downwards, which however still produces a residual settlement at the wall tip. Horizontal subsurface movements (u_x) at a vertical section 'close' to the wall ($x = 13\%H_w$; see Fig. 5f) highly depend on the wall deflection mode, with u_x clearly resembling the shape of δ. On the other hand, the deflection mode does not have much influence on either the vertical or the horizontal displacements at the 'far' vertical section ($x = 100\%H_w$; see Fig. 6e and f), along which u_z and u_x change nearly linearly with depth under all deflection modes.

3.4. Maximum surface movement to wall displacement ratios

The relationship between maximum ground surface movements and maximum lateral displacement of the wall is used as a first design step

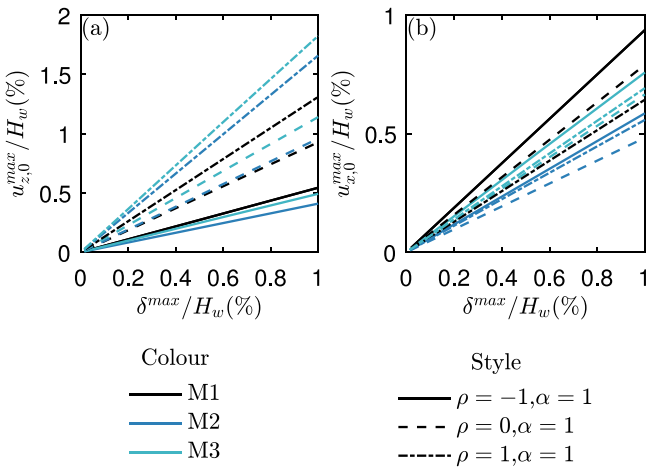

Fig. 7. Ratios between maximum surface ground movements and maximum lateral wall displacement (both normalized by wall height): (a) settlements; (b) horizontal movements.

in practice. Thus, it is of interest to evaluate the predictions of this ratio provided by the proposed method. Fig. 7 presents the ratio between the maximum ground displacements at the surface, $u_{z,0}^{max}$ and $u_{x,0}^{max}$, and the maximum horizontal wall displacement, δ^{max} (note that both are normalized by the wall depth), illustrating the sensitivity of results to the effects of (i) the wall deflection mode (M1 to M3) and (ii) of the ground ovalization ($\rho = -1$, 0 and 1). Figures including M4 results are given in supplemental data. A constant-volume assumption from $\alpha = 1.0$ is employed in all cases.

Fig. 7a shows that surface settlements increase linearly with δ^{max}, but with a widely variable $u_{z,0}^{max}/\delta^{max}$ ratio, that spans from ≈0.4 to ≈1.8; the ratio depends mainly on the value of the ground ovalization parameter, ρ, so that the ratio increases from negative to positive ovalization values. The wall deflection mode also has some influence, although smaller than the influence of ρ; also, note that the influence of the deflection mode depends on the value of ρ: for $\rho = -1$ the largest surface settlements occur for the cantilever (M1) deflection mode, whereas for $\rho = 1$ the largest surface settlements occur for the composite (M3) mode. On the other hand, the impact of the soil relative ovalization on the maximum horizontal displacements of the surface is similar to the influence of the wall deflection mode. As shown in Fig. 7b, negative ρ values and wall deflection modes characterized by displacements of the wall head (i.e., cantilever, M1; and composite, M3 modes) produce the largest $u_{x,0}^{max}/\delta^{max}$ ratios (the $u_{x,0}^{max}/\delta^{max}$ ratios vary from ≈0.47 to ≈0.93 in this case).

3.5. Discussion

This sensitivity analysis demonstrated that (i) ground deformations associated with deep walls are crucially affected by the ground ovalization (which affects both the shape and magnitude of displacement patterns); and (ii) that volumetric strains mainly affect the amplitude of the displacement field, but not (or not so much) its shape. In addition, it demonstrated that soil movements are crucially affected by the lateral displacements of the top part of the wall. Ground displacements for parabolic (M2) and kick-in (M4) wall deflections are similar, with relatively small ground deformations near the wall; while larger maximum movements, and greater displacement gradients with depth, are obtained from the cantilever (M1) or composite deflection model (M3). This has the important practical implication that cantilever (M1) and composite (M3) deflection modes hold the greatest potential for distortions on nearby foundations or infrastructure, and hence for their associated damage.

Similarly, the result also shows that the ratios between maximum ground surface movements and maximum lateral displacement of the wall are also heavily affected by the wall deflection mode and ground ovalization considered. Therefore, solutions that can account for the influence of these aspects are needed, since they could have a relevant practical influence.

4. Comparison with empirical curves

To demonstrate that the proposed analytical method to predict excavation-induced displacements is a reliable alternative to empirical methods, the proposed solution is firstly compared with empirical approaches to estimate surface settlement profiles (Clough and O'Rourke, 1990; Ou et al., 1993; Gaba et al., 2003; Kung et al., 2007a; Mair, 2013); note that this choice is also due to the scarcity of empirical curves for subsurface movements which, when available, (see e.g., Mu and Huang (2016)) are often site-specific. However, to conduct this comparison, the "characteristic excavation depth" should be discussed first; this is because ground movements are often normalized by the excavation depth H in empirical methods, whereas the wall height H_w is the characteristic input length employed in the proposed analytical method. Considering that, for most case studies reported (see e.g., Kung et al., 2007a; Wang et al., 2010), the embedded depth ratio $(H_w - H)/H$ ranged between 0.6 and 1.5, a value of 1.0 (or $H_w/H = 2$) is assumed herein.

All the empirical settlement distributions considered in this paper – which provide the relationship between excavation-induced settlements normalized by the maximum settlements ($u_{z,0}/u_{z,0}^{max}$) as a function of the offset-to-wall depth ratio (x/H_w) – were proposed for excavations in soft and stiff clays. They are summarized in Fig. 8a and b, for spandrel and concave types of settlement distributions, respectively. Fig. 8 distinguishes between best-fit curves (lines with markers) or upper bound envelopes (lines only) obtained from multiple case studies; the layout also indicates whether they apply to soft clays (dark colour) or to stiff clays (light colour). Overall, the empirical curves considered indicate a wide range of expected surface settlements, with best-fit profiles (Ou et al., 1993; Kung et al., 2007a) being narrower than upper bound envelopes (Gaba et al., 2003; Clough and O'Rourke, 1990); in other words, and as expected, 'best fit' curves provide smaller surface settlements than 'upper bound' curves. Next, the empirical curves considered are compared with the analytical predictions provided by the proposed method, considering both the effects of ground ovalization and of the wall deflection mode.

Fig. 9 compares the empirical curves for vertical and horizontal excavation-induced movements in stiff clays with the corresponding analytical predictions; note that both surface movement and distance from the wall were normalized by wall height in Fig. 9. As empirical curves, the design envelopes for stiff clay of Mair (2013) and Gaba et al. (2003) (for propped 'stiff walls' and for anchored sheet pile walls or 'flexible walls') were selected. Two deflection modes of the wall (M1 and M3) and three ovalization values ($\rho = -1, 0$ and 1) are used as input in the proposed analytical method, hence allowing us to identify which combination of ground ovalization and wall deflection mode provides a better fit to the empirical envelopes. Note that a different level of wall deflection β is associated with each empirical settlement envelope, on the assumption that the wall deflection area is approximately equal to the settlement area under undrained conditions ($\alpha = 1$). From this, three wall deflection levels ($\beta = 0.036\%, 0.043\%$ and 0.129%) were selected.

'Stiff wall' systems, that are associated with a 'low' displacement level or 'low' β value, are addressed first, as shown in Fig. 9a. For this case, the empirical $u_{z,0}$ suggests a concave-type settlement trough, which is more closely matched using the composite (M3) deflection mode and a negative ovalization ($\rho = -1$); however, the analytical method predicts smaller settlements close to the wall, due to the analytical troughs being wider than the envelopes.

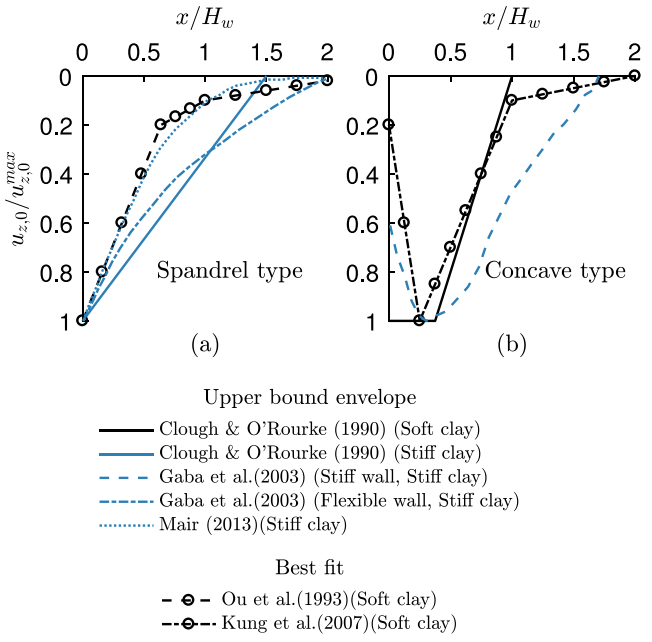

Fig. 8. 'Upper bound' and 'best fit' empirical settlement curves: (a) spandrel and (b) concave type.

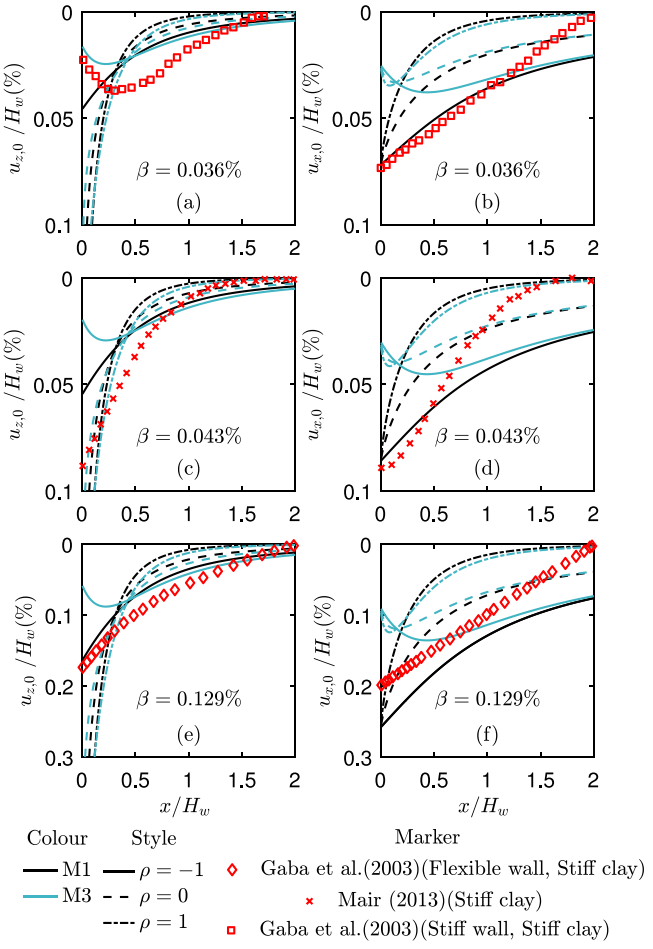

Fig. 9. Comparison between (i) analytical predictions of horizontal and vertical surface movements (ii) and empirical upper-bound envelopes proposed by: (a)–(b) Gaba et al. (2003) for flexible walls in stiff clay; (b)–(c) Mair (2013) for stiff clays; (e)–(f) Gaba et al. (2003) for stiff walls in stiff clays.

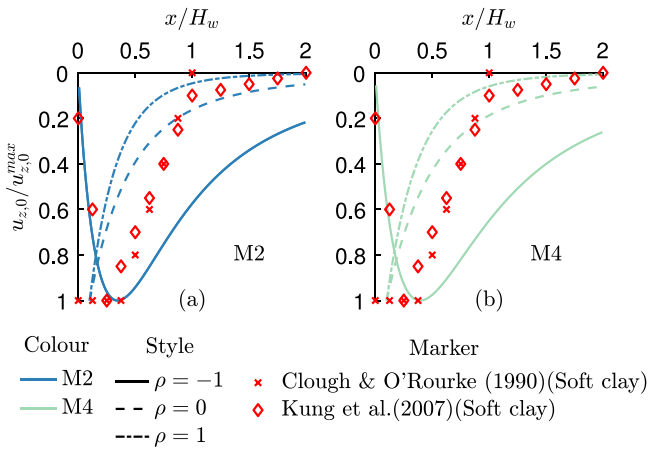

Fig. 10. Comparison of (i) predicted surface settlements and (ii) concave-type empirical surface settlement distributions (for soft clays).

Then, the empirical spandrel-type settlement distribution suggested by Mair (2013) and Gaba et al. (2003) for 'flexible walls' are discussed (see Fig. 9c and e). The anchored sheet pile walls in Fig. 9e give the largest displacement levels, β, as expected. The empirical envelope of Mair (2013) is reasonably predicted by both M1 and M3 deflection modes, assuming no ovalization ($\rho = 0$); whereas the envelope for 'flexible walls' by Gaba et al. (2003) can be reproduced under M3 assuming $\rho = -1$. Surprisingly, Fig. 9b shows that upper-bound empirical horizontal surface movements $u_{x,0}$ are well predicted by the cantilever deflection mode (M1) for ovalization values between $\rho = -1$ and 0, in all cases, whereas a concave distribution is associated with the composite M3 deflection. The fact that different modes would provide the best match is likely due to the 'envelope' nature of these empirical curves.

Next, we discuss the analytical inputs that the analytical model requires, so as better to capture the features of concave vs spandrel-type shapes. Figs. 10 and 11 compare the analytical predictions (normalizing settlements by their maximum value, $u_{z,0}/u_{z,0}^{max}$, hence making results independent of the β value considered) against the empirical curves. Note that, for spandrel-type settlement profiles, the analytical result shows a relatively large value near the wall, which is unrealistic. Thus, $u_{z,0}^{max}$ of spandrel-type settlement distributions is inferred from the location of $x = 0.1\%H_w$ in this section.

Fig. 10 compares results for concave-type settlement profiles, as often observed for braced excavations in soft to medium clays (Clough and O'Rourke, 1990; Kung et al., 2007a). This type of profile can be captured by the parabolic (M2) and kick-in (M4) wall deflection modes, assuming a negative ovalization ($\rho = -1$); note that this combination reproduces both (i) the location of the maximum ground settlement and (ii) the distribution of settlements close to the wall. However, the analytical solution is wider than the empirical ones, overpredicting settlements far away from the wall.

Fig. 11 compares results for spandrel-type surface settlement profiles: Clough and O'Rourke (1990) suggested an empirical triangular settlement distribution for deep excavations in stiff clay; whereas Ou et al. (1993) proposed a trilinear line for excavations in soft clay. In each subplot, these empirical profiles are compared against analytical results for a specific wall deflection mode (M1-M4). As shown in Fig. 11a and c, the profile of Clough and O'Rourke (1990) (for stiff clay) can be reasonably reproduced by the cantilever (M1) and composite (M3) deflection modes, using $\rho = -1$, while the parabolic (M2) and kick-in (M4) modes are narrower, underestimating the settlement envelopes of Clough and O'Rourke (1990) (see Fig. 11b and d). The profile of Ou et al. (1993) (for deep walls in soft clay) can be best reproduced, for all deflection modes (M1 to M4) using a null ovalization ($\rho = 0$).

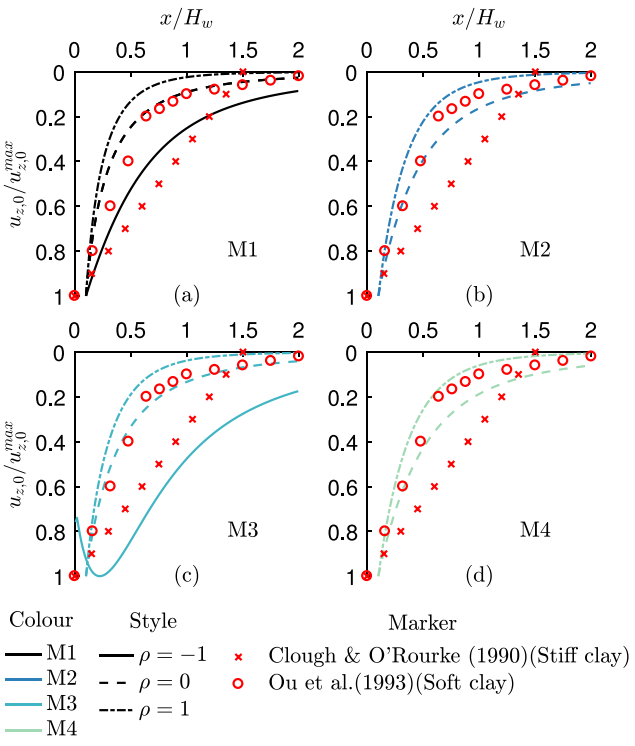

Fig. 11. Comparison of (i) predicted surface settlements and (ii) spandrel-type empirical surface settlement distributions (for soft to stiff clays).

The comparison with empirical envelopes suggests that the proposed analytical solutions can rationally describe the surface ground movements, in both vertical and horizontal directions. Note, however, that different soil ovalization values may be required to better reproduce different ground conditions, or different wall construction methods and bracing configurations (which affect the wall deflection mode).

5. Comparison with field and experimental case studies

To evaluate the applicability of the analytical prediction method in practice, ground movements measured in well-known case histories of braced excavations in varying ground conditions (Miyoshi, 1977; Burland and Hancock, 1977; Finno et al., 1989; Ou et al., 1993; Hsieh and Ou, 1998; Ng, 1998; Kung et al., 2007b; Ng et al., 2012; Khoiri and Ou, 2013; Korff et al., 2016) are considered. Additionally, the centrifuge tests conducted by Ng et al. (2017) and Lam et al. (2014) in dry sand and clay, respectively, are also analysed to consider ideal ground conditions and controlled boundary conditions. Table 1 summarizes all case studies and centrifuge tests, detailing the final excavation depth and the wall length, the maximum wall deflection and ground surface movements, and the ratio between surface ground loss and wall ground loss.

5.1. Maximum surface movements

Fig. 12 compares the analytical predictions of maximum surface movements with field and centrifuge data of the case histories considered. For simplicity, only analytical data inferred from the parabolic (M2) wall deflection mode are reported in this figure, since they are nearly identical to results for the kick-in (M4) mode (see Fig. 7). Also, note that logarithmic scales are used in Fig. 12 to better display results at small wall deflection levels; and that analytical results are computed for constant-volume conditions ($\alpha = 1$).

Table 1
Excavation case studies.

#	Case	H (m)	H_w (m)	δ^{max} (mm)	$u_{z,0}^{max}$ (mm)	$u_{x,0}^{max}$ (mm)	β (%)	$V_{l,s}/V_{l,w}$	References	Soil condition	Final mode
1	TNEC	19.7	35	106	78	40	0.19	0.79	Ou et al. (1998)	Soft clay	M2
2	Formosa	18.5	31	61	42	N/A	0.12	0.74	Ou et al. (1993)	Soft clay	M2
3	Far-Eastern	20	33	124	79	N/A	0.24	N/A	Hsieh and Ou (1998)	Soft clay	M3
4	Tokyo subway	17	32	175	154	N/A	0.31	1.29	Miyoshi (1977)	Soft clay	M2
5	GuBei Station	14.5	26	46	47	N/A	0.03	1.97	Ng et al. (2012)	Soft clay	M2
6	HDR-4	12	19	190	256	N/A	0.53	N/A	Finno et al. (1989)	Soft clay	M2
7	Centrifuge (T2)	5.14	9.6	99	101	N/A	0.77	0.81	Lam et al. (2014)	Soft clay	M4
8	Centrifuge (T3)	5.14	9.6	65	72	N/A	0.41	1.06	Lam et al. (2014)	Soft clay	M2
9	Centrifuge (T5)	5.14	9.6	99	75	N/A	0.68	0.78	Lam et al. (2014)	Mix	M2
10	N.P.Yard Park	18.5	30	24	19	14	0.05	N/A	Burland and Hancock (1977)	Stiff clay	M4
11	Lion yard	10	17	13	10	8.5	0.06	1.23	Ng (1998)	Stiff clay	M3
12	O6 station	19.6	36	55	28	N/A	0.09	0.97	Khoiri and Ou (2013)	Sand	M4
13	O7 station	21.7	38	66	20	N/A	0.09	0.73	Khoiri and Ou (2013)	Sand	M4
14	Ceintuurbaan St.	26	44	20	11	N/A	0.02	0.90	Korff et al. (2016)	Mix	M4
15	Centrifuge test	8	12	15	13	N/A	0.10	N/A	Ng et al. (2017)	Sand	M3

Real settlement data in Fig. 12a are within a range of $u_{z,0}^{max}/\delta^{max} \approx$ 0.3 to ≈1.35, associated with observations that normally are bounded by the analytical predictions corresponding to ovalization levels of $\rho = -1$ to $\rho = 0$. This suggests that such ovalization levels ($\rho = -1$ to $\rho = 0$) are likely under similar field conditions, whereas $\rho = 1$ situations are unlikely. Importantly, this observation that $\rho = 1$ is not suitable to replicate empirical evidence was also drawn in the previous section, from our comparison with the empirical surface settlement curves (see Figs. 9–11). Also, Fig. 12b illustrates the ratio between the maximum horizontal ground displacement and the maximum horizontal wall displacements, for the few available case histories that report such data. It can be observed that the analytical predictions of the $u_{x,0}^{max}/\delta^{max}$ ratio are not far from the field observations. Finally, results are plotted in linear scale against the 1:1 line in Fig. 12c and d.

5.2. Case studies in clay

5.2.1. New Palace Yard Park in London from Burland and Hancock (1977)

The deep excavation for the New Palace Yard Park in stiff London clay had an excavation depth $H = 18.5$ m, supported by a diaphragm wall with $H_w = 30$ m and five levels of struts. Surface ground movements and the wall deflection were monitored. A relatively low average wall displacement ($\beta = 0.05\%$) was achieved, which is consistent with typical empirical values for stiff clays and stiff (braced) walls; see Fig. 9.

Fig. 13 shows the deflection along the wall (used as input), and the comparison between observed and predicted ground movements along the ground surface. Analytical results are computed for incompressible soil ($\alpha = 1$) and varying ovalization levels. Vertical and horizontal movements in Fig. 13b and c obtained for no ovalization ($\rho = 0$) provide the best-fit to field monitoring data, also providing a reasonable approximation to the distribution of field movements. On the other hand, solutions for $\rho = -1$ tend to underestimate the vertical soil displacements close to the wall. The fact that the analytical predictions using $\rho = 0$ performed better is likely due to the counteracting effects of effective braced support (leading to a small β with a value of 0.05%) and a high coefficient of earth pressure at rest. Importantly, analytical predictions for $\rho = 0$ satisfy the empirical observation by Clough and O'Rourke (1990) that, for stiff clay, a spandrel-type surface settlement distribution is expected.

5.2.2. Lion yard from Ng (1998)

The works at the Lion yard site in Cambridge involved a 10 m deep excavation in stiff gault Clay supported by a concrete diaphragm wall with $H_w = 17$ m and four levels of struts. Surface ground movements monitored at Panel 22 and reported by Ng (1998) are considered. A relatively small wall displacement level (of $\beta \approx 0.05\%$ to ≈0.06%) was also achieved during the main excavation in this case history in stiff soil.

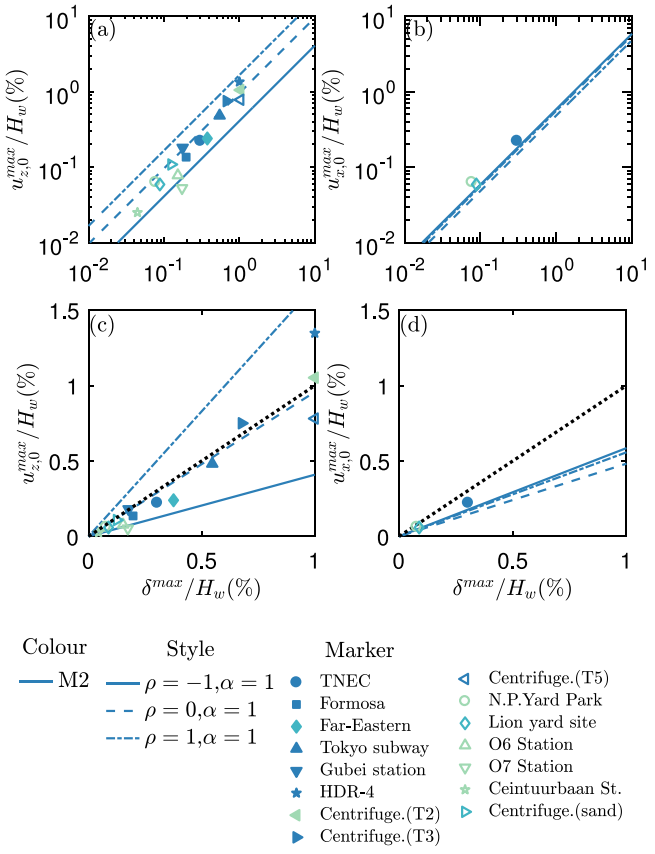

Fig. 12. Comparison between analytical and field/experimental data of maximum vertical and horizontal ground displacements at the surface, as a function of the maximum wall deflection, in (a)–(b) logarithmic and (c)–(d) linear scale.

Fig. 14 displays measured wall deflections (also used as inputs); and it compares computed and recorded surface movements. Analytical computations were conducted assuming incompressible ground, or $\alpha = 1$, and the composite wall deflection mode (M3) was employed based on this case. A concave-type settlement profile occurred in the field after the completion of the main excavation stage (see Fig. 14b), which can be adequately predicted using a negative ovalization ($\rho = -1$), despite the resulting slight settlement underestimation; also, the monitored horizontal displacements $u_{x,0}$ were reasonably replicated. Ng (1998) suggested that the settlement distribution $u_{z,0}$ resembled a concave-type distribution (as for excavations in soft clays) rather than spandrel-type distribution, and that this was likely due to the adopted construction

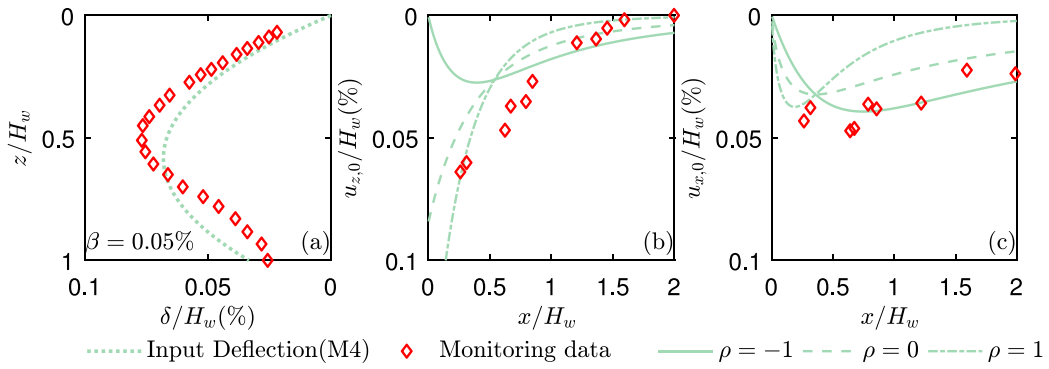

Fig. 13. Measurements and predictions in stiff London clay (Burland and Hancock, 1977): (a) wall deflection; (b) vertical and (c) horizontal displacements at the surface.

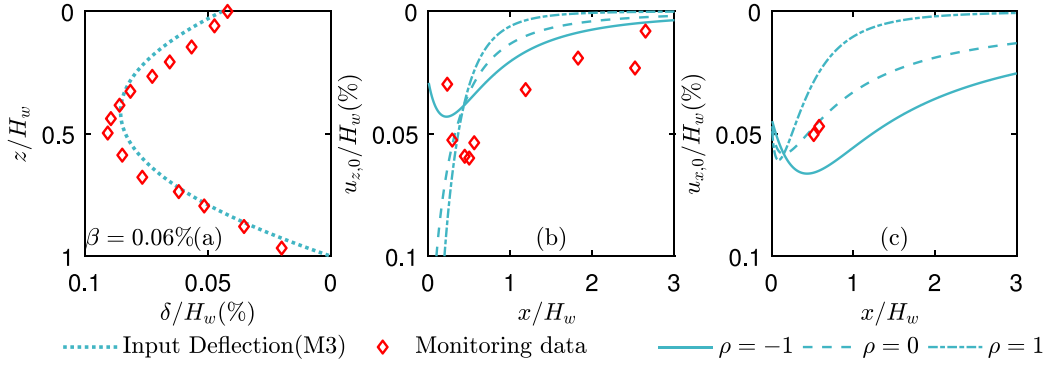

Fig. 14. Measurements and predictions for the Lion Yard site in stiff gault clay (Ng, 1998): (a) wall deflection; (b) surface settlements and (c) surface horizontal displacements.

method. Interestingly, this field observation suggests that the construction method could affect the type of settlement distribution, while analytical predictions indicate that this effect could be captured by an adequate selection of the ovalization term, ρ (with $\rho = 0$ producing for spandrel-type distributions and $\rho = -1$ producing more concave-type distributions).

5.2.3. Taipei National Enterprise Center reported by Ou et al. (1998) and Kung et al. (2009)

Field observations from the Taipei National Enterprise Center (TNEC) are of interest to analyse the behaviour of excavations conducted in soft silty clay. This case is particularly interesting because inclinometers were installed to monitor subsurface horizontal movements u_x at $x = 2$, $x = 8$ and $x = 16$ m from the wall. A diaphragm wall with $H_w = 35$ m and a 0.9 m thickness was used to conduct this excavation with $H = 19.7$ m height, which was supported by five concrete slabs; this design produced a medium deflection level ($\beta = 0.19\%$) of the wall after its excavation. Fig. 15 reports the horizontal displacements at the wall and at the inclinometer locations, for two excavation stages (Stages 5 and 13). Surface movements are plotted in Fig. 16.

Fig. 15a shows that, at Excavation Stage 5 ($H = 8.6$ m), the composite deflection mode (M3) reproduces well the wall movements, with a (still) relatively small deflection level ($\beta \approx 0.07\%$). However, the deflection mode changed as the excavation progressed so that, at the final excavation stage (Stage 13, for $H = 19.7$ m; see Fig. 15e) the average deflection level had increased significantly (up to $\beta \approx 0.19\%$), and the parabolic deflection mode (M2) had become dominant. Therefore, the corresponding deflection mode (M3 or M2) is selected as an input, accordingly. Also, $\alpha = 1$ is assumed in all cases.

Fig. 15b–c show that, at Excavation Stage 5, subsurface horizontal ground movements at the 'close' and 'mid-distance' inclinometers are well described by the analytical method using $\rho = -1$. However, the analytical predictions with $\rho = -1$ slightly overestimate the horizontal displacements at the 'far' section, which are better reproduced by $\rho = 0$ in Fig. 15d. These same trends can also be observed for Excavation Stage 13 in Fig. 15f–h. The main differences between field measurements and the analytical results are due to the analytical overestimation of horizontal ground movements at the wall tip depth ($z = H_w$), especially at the 'far' section.

Next, Fig. 16 shows surface ground movements at different stages of the TNEC excavation. Note that the analytical results near the wall are too large when no ovalization is considered and that the distribution of surface settlements $u_{z,0}$ are well predicted using $\rho = -1$ at Excavation Stage 5. Also the location of the maximum settlement $u_{z,0}^{max}$ is reasonably captured by the prediction method using $\rho = -1$ at Excavation Stage 13; however, at this stage, the analytical solution underestimates the surface settlements measured, particularly near the wall (i.e., for $x \leq 0.75H_w$). Contrarily, horizontal surface movements $u_{x,0}$ are well described close to the wall, while they are likely overestimated far from it. Note also that $\rho = 0$ seems to provide a better fit in this case.

This case study highlights one limitation of the proposed model, due to the assumption of elastic material and incompressible soil: such a model cannot capture the distribution of ground displacements close to the wall for medium-to-large wall deflection levels, which are probably associated with non-elastic behaviour. Similar conclusions are obtained after analysing the field data of the HDR-4 pit construction in Chicago soft clay (Finno et al., 1989), which were associated with large β values (see the supplemental data). Semi-empirical correction factors could be introduced to consider this phenomenon, similar to those proposed by Loganathan and Poulos (1998) for tunnelling; however, this is beyond the scope of this work.

5.2.4. Centrifuge tests in kaolin clay (Lam et al., 2014)

Centrifuge tests were carried out by Lam et al. (2014) to study the undrained response of deep excavations in overconsolidated (medium-stiffness) clays. The model wall consisted of an aluminium plate, simulating sheet piles or a diaphragm wall, with a prototype height of

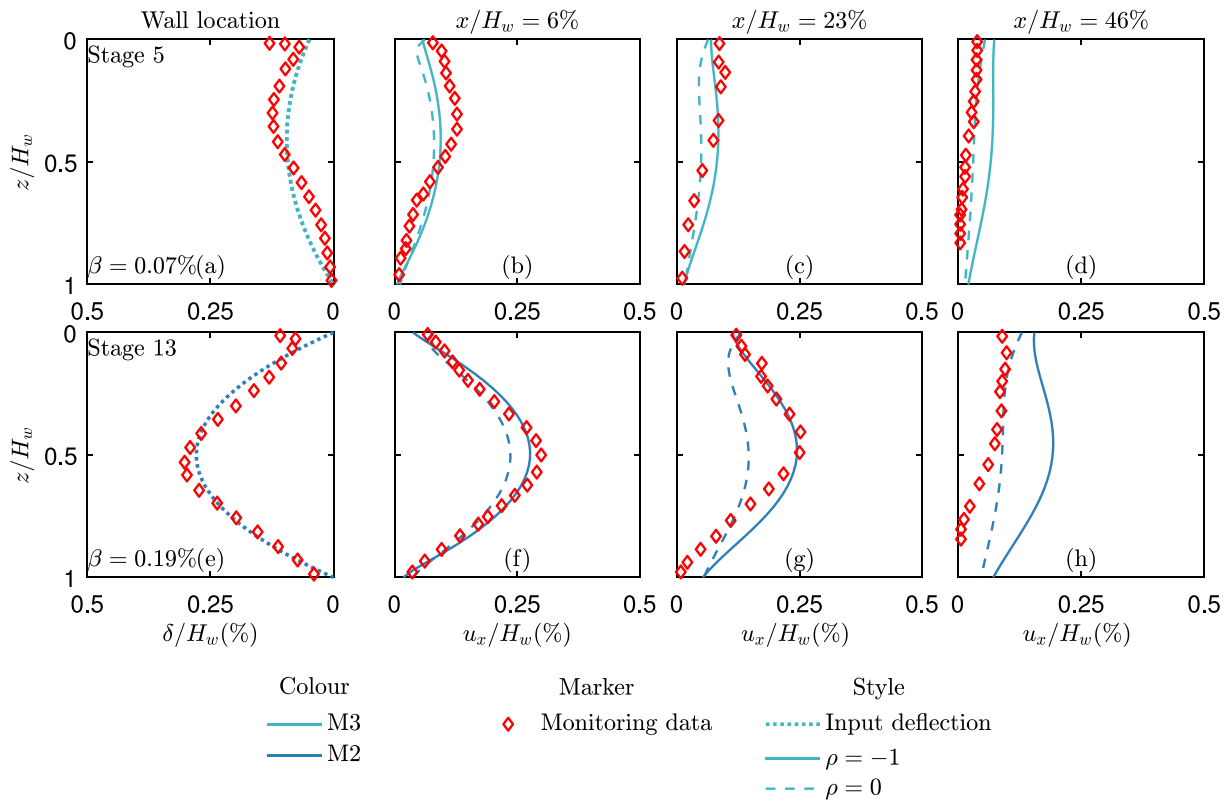

Fig. 15. Soil horizontal subsurface movements from the TNEC case in soft clay (Ou et al., 1998; Kung et al., 2009).

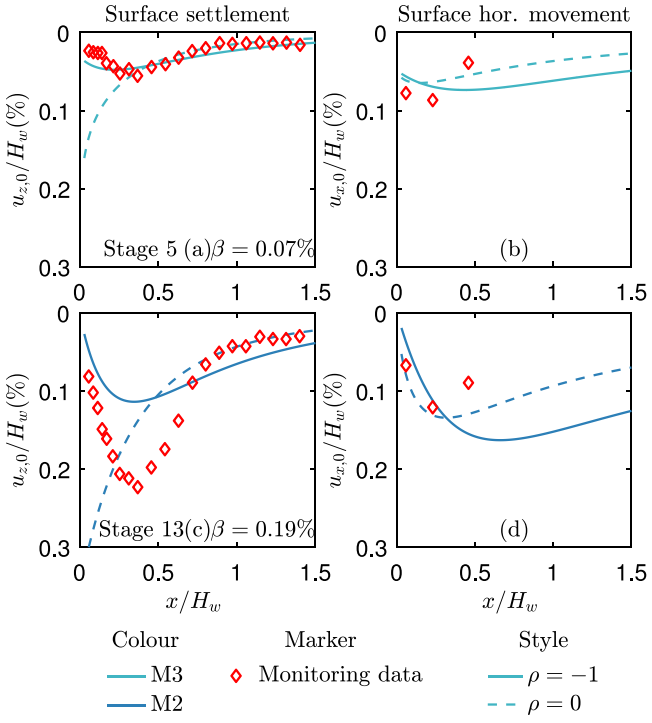

Fig. 16. Ground surface settlements and horizontal movements from the TNEC case in soft clay (Ou et al., 1998; Kung et al., 2009).

H_w = 9.6 m and with three levels of props. Both the intermediate (Stage 2, after installing the second prop; with $H/H_w = 0.23$ for Test 2 and $H/H_w = 0.35$ for Test 3) and final (Stage 3; for $H/H_w = 0.54$) excavation stages are considered. Based on their observed deformation profiles, Centrifuge Tests 2 and 3 are considered to initially have the wall tip free and fixed, respectively, corresponding to composite (M3) and parabolic (M2) deflection modes; see Fig. 17a and c. However, note that in Test 2 the wall tip started to move during Stage 3, this suggests a kick-in (M4) deflection mode for this later Stage. Due to the soil shearing, horizontal displacements were induced beneath the wall; however, these displacements beneath the tip are neglected because the associated volume loss is less than 10% the area associated with the wall deflection (see Fig. 17b).

Fig. 17a–d summarizes the experimental wall deflection δ and the selected analytical inputs employed to compute the analytical predictions. A parabolic deflection (M2) mode is employed to capture the behaviour of the wall with a fixed head and tip, as observed in Test 3; whereas in Test 2, a composite (M3) deflection mode is employed for Stage 2, and a kick-in (M4) mode is employed at its final stage (Stage 3). The corresponding surface ground settlements are shown in Fig. 17e–h; note that the results predicted close to the wall ($x < 0.5$ m) are not plotted.

Fig. 17e–f and g–h show the evolution of surface settlements as the tests progressed. The settlement distribution at the intermediate excavation stage is well predicted by the solution with null ovalization ($\rho = 0$), which provides a spandrel-type settlement distribution (it does, however, not capture the small concave profile close to the wall; see Fig. 17e and g). Similarly, the analytical predictions with $\rho = 0$ are also representative of measurements conducted at the final excavation stage, which in this case are associated with high wall deflections ($\beta \approx 0.77\%$ and $\approx 0.41\%$ for free and fixed tip, respectively) produced due to the high stress relief that occurred in the model tests before installation of the first prop. The likely reasons why these results do not align with previous experience are discussed in the discussion section.

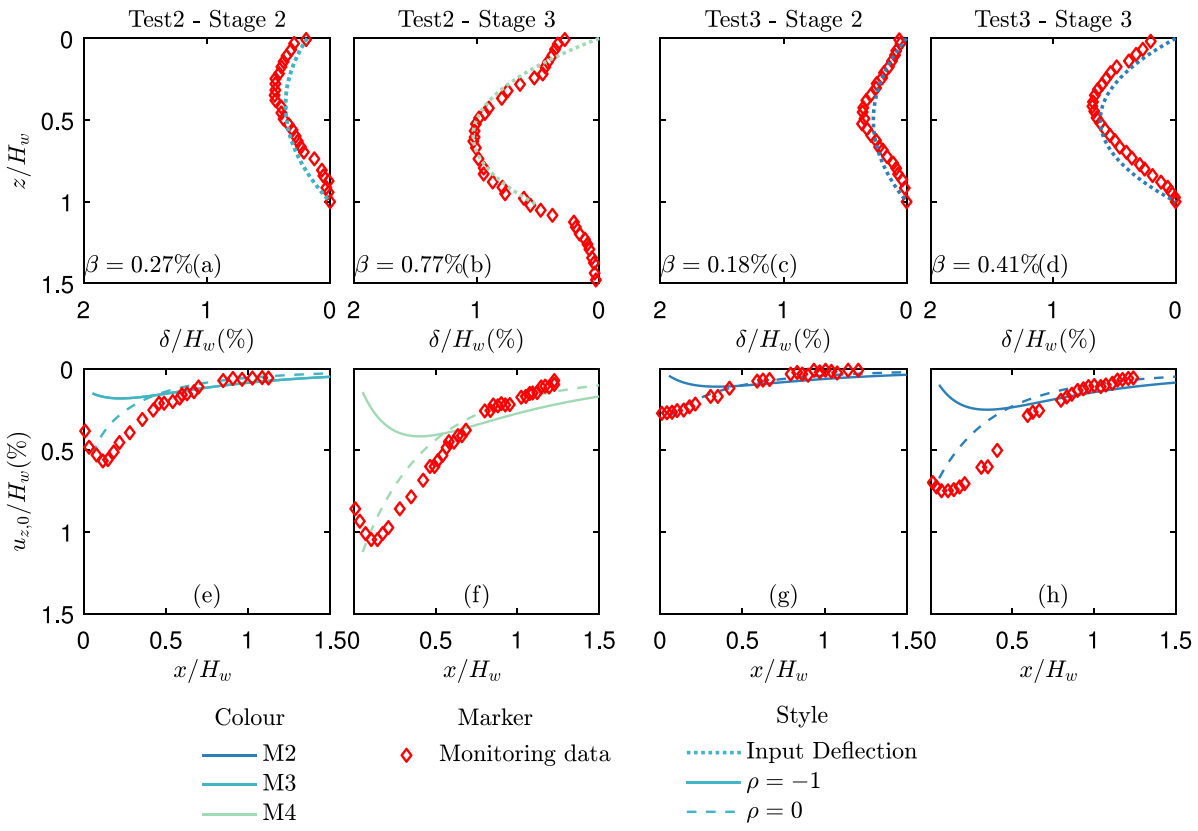

Fig. 17. Wall deflections and surface settlements from prediction and centrifuge tests in clay (Lam et al., 2014): wall deflection at the intermediate (Stage 2) and final (Stage 3) stage for free (a)–(b) and (c)–(d) fixed wall tip; surface settlements at the intermediate (Stage 2) and final (Stage 3) stage for free (a)–(b) and (c)–(d) fixed wall tip.

5.3. Case studies in sand

5.3.1. Kaohsiung O6 station from Khoiri and Ou (2013)

The deep excavation for Station O6 of the Kaohsiung Rapid Transit System – conducted in silty sand with some thin clay layers – is considered next. The final excavation depth was $H = 19.6$ m, and diaphragm walls of $H_w = 36$ m height and 1.0 m thickness were used, which were supported with five levels of W-section steel struts. This resulted in a relatively low deflection level of $\beta = 0.09\%$.

To account for the possibility of volume change (associated with drained sand behaviour), the excavation-induced volumetric strains are accounted for through the α parameter employed in the proposed solution. To span across dilative and contractive behaviour, $\alpha = 0.97$ and 1.02 are adopted, along with $\rho = 0$ and $\rho = -1$ ovalization values. The final wall deflection is approximated by the kick-in (M4) deflection mode, although this mode does not fully reproduce the real deflection shape, as shown in Fig. 18a. Note that our analytical approach can be employed with any given distribution of δ and indeed we present the results corresponding is a curve-fit approach as supplemental data. However, the improvement of results is not always relevant, so the same approach employed so far was maintained, based on analyses produced using one of the four fundamental deflection modes (M1 to M4) considered in Fig. 3. Fig. 18b displays the surface settlement measured at the final excavation stage, and compares them with several predictions of the analytical method. Results show that the field measurements are better predicted by the analytical solution with $\alpha = 0.97$ and $\rho = -1$; that is, with the analytical solution associated with contractive strains and negative ovalization. In contrast, the spandrel-type settlement profile predicted when a null ovalization was used does not seem to be realistic in this case, once it is compared with the available field measurements.

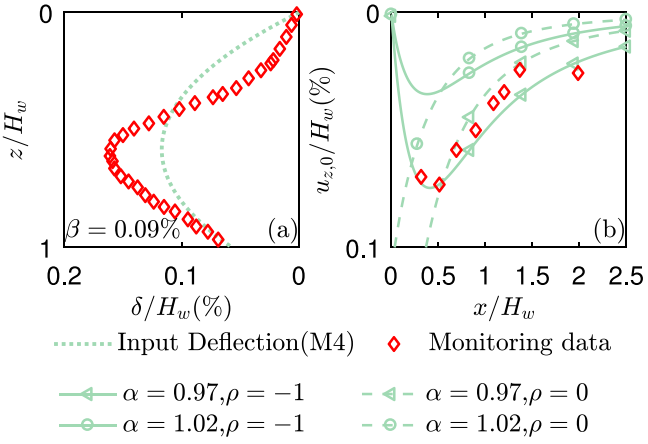

Fig. 18. Field displacements in sand (Khoiri and Ou, 2013): (a) wall deflection and (b) surface settlements.

5.3.2. Centrifuge test in sand (Ng et al., 2017)

As a final case study, the centrifuge test of a multi-propped excavation in dry Toyoura sand with a 70% relative density is considered. At prototype scale, the final excavation depth reached a height of $H = 8$ m, which was supported by a diaphragm wall with height $H_w = 12$ m supported by two levels of props, located $z = 1$ and $z = 5$ m beneath the surface. Surface settlements $u_{z,0}$ and vertical u_z and horizontal u_z ground movements were measured at an offset of $x = 3$ m from the wall. On the other hand, since wall deflections were not measured during the experiments, the wall deflection computed numerically by Ng et al. (2017) is selected as the input of the proposed numerical approach.

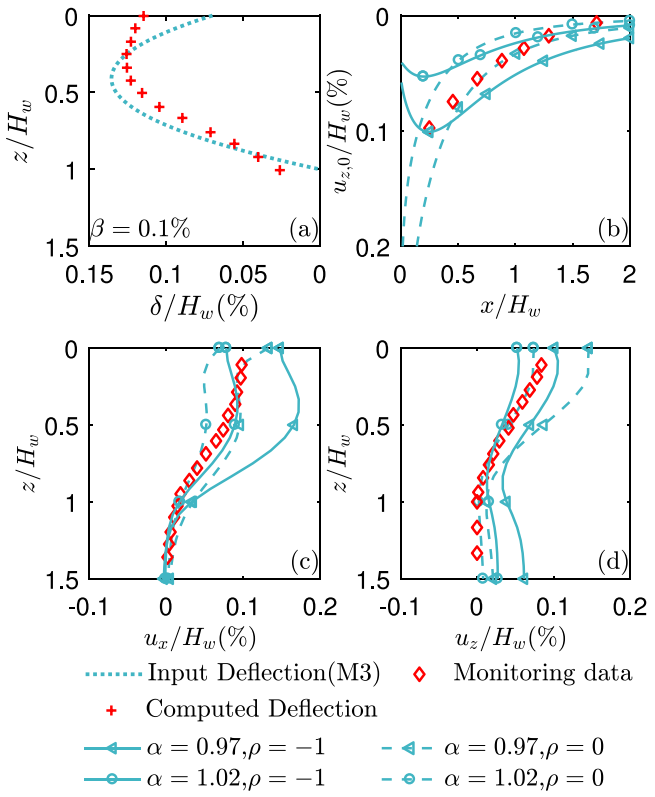

Fig. 19. Centrifuge displacements in sand (Ng et al., 2017): (a) wall deflection, (b) surface settlement, (c)–(d) subsurface movement along the vertical section at $x = 3$ m ($25\%H_w$).

Analytical predictions are computed using two different volumetric parameters ($\alpha = 0.97$ and 1.02) and two ovalization cases (no ovalization, $\rho = 0$; and negative ovalization, $\rho = -1$). The predicted soil movements are compared with the centrifuge measurements in Fig. 19, with results showing that the wall deflection profile at final excavation can be adequately reproduced using the composite (M3) deflection mode (see Fig. 19a). Fig. 19b indicates that (except for locations close to the wall) the spandrel-type surface settlement profile is better captured by the analytical method using no ovalization ($\rho = 0$), and with a slight contractive soil behaviour ($\alpha = 0.97$). This agrees with experiments of tunnelling in medium-dense sand that displayed an average contractive volumetric response for small volume losses (Franza et al., 2019). On the other hand, using negative ovalization ($\rho = -1$) and contractive behaviour ($\alpha = 0.97$) can only capture the surface settlements close to the wall, but at the expense of producing an overall surface settlement trough that is wider than measured. Fig. 19c and d show the vertical and horizontal subsurface movements at an offset of $x = 3$ m from the wall. Subsurface displacement results agree with measured horizontal subsurface movements, whereas the analytical results slightly overestimate the vertical subsurface movements, when no ovalization and contractive behaviour are assumed. Considering together all (i.e., both surface and subsurface) prediction results, it is argued that a slight contraction behaviour and an intermediate negative ovalization (say, of $\rho = -0.5$) seems preferable in this case.

6. Discussion of the relative ground ovalization

In this method, ground ovalization plays an important role in both the distribution and magnitude of ground displacements. To help engineers to use the proposed analytical method (e.g. selecting the relative ovalization value as a function of wall deflection level, wall deflection mode, and ground conditions), Table 2 summarizes the ovalization ρ inferred from the case histories analysed in this paper with engineering judgement; the corresponding chart is provided in supplemental data. The following indications are drawn.

Table 2
Relationship between wall displacement level β and relative ovalization ρ, considering soil type and wall deflection mode (see Table 1 for description of case histories).

#	Case	β (%)	ρ	Soil condition	Final mode
5	GuBei Station	0.03	−0.75	Soft clay	M2
2	Formosa	0.12	−1	Soft clay	M2
1	TNEC	0.19	−1	Soft clay	M2
3	Far-Eastern	0.24	−0.25	Soft clay	M3
4	Tokyo subway	0.31	−1	Soft clay	M2
8	Centrifuge (T3)	0.41	0	Soft clay	M2
6	HDR-4	0.53	−0.75	Soft clay	M2
7	Centrifuge (T2)	0.77	0	Soft clay	M4
10	N.P.Yard Park	0.05	0	Stiff clay	M4
11	Lion yard	0.06	−0.75	Stiff clay	M3
12	O6 station	0.09	−1	Sand	M4
13	O7 station	0.09	−1	Sand	M4
15	Centrifuge test	0.10	−0.5	Sand	M3
14	Ceintuurbaan St.	0.02	−1	Mix	M4
9	Centrifuge (T5)	0.68	−0.5	Mix	M2

- Contrarily to tunnelling, positive ovalization of the ground in this analytical model is unlikely for deep excavations; $\rho = 0$ is suggested as an upper threshold for sensitivity studies.
- In stiff clay, it is important to consider how the construction method impacts the expected wall deflection mode for low wall deflection levels β (say, $\beta < 0.1\%$).
  - For braced excavations relative ovalization values $\rho \approx of -0.5$ to 0 should be employed when the support system leads to parabolic (M2) and kick-in (M4) type wall deflections. In particular, this relative ovalization level is associated to the empirical curve of spandrel-type surface settlements of Clough and O'Rourke (1990) (see the parabolic (M2) wall deflection mode in Fig. 11) as well as to the monitoring data from the New Palace yard park case study of Burland and Hancock (1977) (associated with the kick-in (M4) wall deflection mode). For M2 and M4 wall deflections, nearly null ovalization values probably occur because of ground losses mainly localized at the wall's mid-depth and because the high coefficients of earth pressure typically associated with stiff clay leads to similar stress relief in the vertical and horizontal directions.
  - The case history in stiff clay from Ng (1998) suggests that construction methods that produce a composite (M3) or a cantilever (M1) wall deflection mode (say, because the wall is unsupported, or because it has a low stiffness support during the initial excavation stages) can lead to a large negative ovalization ($\rho \approx -0.75$ to -1), that tends to be associated with concave-type surface settlement distribution. This is probably because, for a composite deflection mode, more ground losses are localized near the surface, and they tend to be dominated by horizontal soil stress relief. Based on this argument, ρ may tend towards -1 for a cantilever (M1) mode while it may be assumed as -0.75 for a composite (M3) mode.
- Braced excavations in soft clays, sands, and mixed conditions are associated with a wide range of negative relative ovalization values (ρ between -1 to -0.25) when the wall deflection level is expected to be relatively small (say, $\beta < 0.1\%$). Note that the wall deflection mode also plays a role, as follows:
  - Parabolic (M2) and kick-in (M4) modes are associated with ρ between -1 to -0.75 in the case studies considered; this is

because the stress relief in the horizontal direction is more significant than in the vertical direction.
  - Composite (M3) wall deflection resulted in ρ between −0.5 to −0.25.

- Interestingly, the relative ovalization ρ in soft clays for parabolic (M2), composite (M3), and kick-in (M4) wall deflection modes tends towards null values as the wall deflection level β increases to relatively large values (say, $\beta > 0.3\%$) (Lam et al., 2014; Hsieh and Ou, 1998). In particular, centrifuge results of Lam et al. (2014) do not always seem to agree with patterns observed for monitoring data from real projects; this "outlier" trend could also be due to high overconsolidation ratios reported by these authors for the upper part of the clay sample, as a result of sample preparation. This increased the coefficient of earth pressure of the sample before the excavation was simulated, making the subsequent wall excavation produce an unrealistically high horizontal stress release. In conclusion, there are still uncertainties on the relative ovalization ρ at high wall deflection levels, at which the proposed analytical solution may not be applicable.

7. Conclusions

This paper presented an analytical method to predict surface and subsurface ground (horizontal and vertical) movements induced by a deep excavation in sand and clay when the wall deflection is assumed as a model input. To calculate these movements during intermediate and final stages of the excavation, the superposition of cavities is used for the wall deflection while the cavity-induced displacement fields are predicted with the method of González and Sagaseta (2001). This allows one to account for the influence on ground movements of (i) the wall deflection mode – e.g., cantilever, parabolic, composite, or kick-in –; (ii) the ground ovalization behaviour; and (iii) the soil volumetric (dilative or contractive) behaviour. The following conclusions can be drawn.

- The predictions of the analytical method compared well with field data, both in terms of maximum surface movement-to-wall deflection ratios as well as surface settlement shapes (as described by frequently adopted empirical curves). Therefore, the proposed method can serve as a simple tool for the analysis of excavation-soil–structure interaction, when the shape and magnitude of the wall displacement profile is (i) selected based on preliminary predictions from design charts, (ii) matched to excavation monitoring data, or (iii) designed to satisfy an allowable level of ground deformations. In particular, nonlinear distributions of subsurface displacements (as observed in field and experiments) can be obtained close to the wall using this prediction method, depending on the wall deflection and soil ovalization level. This greenfield displacement field, implemented as input of soil-foundation interaction models, can overcome the limitations of design assumptions relying on simplistic subsurface movement distributions; e.g., solving Korff et al. (2016) and Franza et al. (2021) excavation-pile-soil interaction models for subsurface settlements other than linearly decreasing with depth.
- The ground ovalization parameter ρ plays an important role in affecting the magnitude and shape of surface and subsurface movements induced by deep excavations. The value of ρ to be employed depends on both the wall deflection mode and the soil condition, with wall deflection level playing a minor role at low β values (say, $\beta < 0.1\%$). On the other hand, the volumetric parameter α only influences the magnitude of the excavation-induced displacements, with little effect on their distribution shape. Field evidence indicated that coarse-grained soil may undergo average contractive behaviour as the result of deep excavations and, thus, α values lower than unity may be adopted to conservatively estimate the magnitude of the associated movements.
- The soil movements, both at the surface and the subsurface, are significantly affected by the wall displacement profile, particularly for the subsurface distributions. Cantilever, parabolic, composite, and kick-in deflection modes were analysed. Everything else being equal, the maximum surface movement is minimum under the kick-in mode and maximum under the cantilever mode. A hogging-type deformation occurs for the settlement trough associated with the cantilever wall mode, regardless of the value of the relative ovalization parameter. For the other three wall deflection modes (parabolic, composite, and kick-in), a sagging zone is developed close to the wall and then it is followed by a hogging zone at a greater distance only in the presence of a negative soil ovalization term, whereas hogging profiles are obtained for null soil ovalization. Thus, both wall deflection mode and soil ovalization have a significant effect on the maximum curvature of the settlement profile and on the location of the inflection point, which both affect the potential for distortions of near foundations and infrastructure.
- The comparison with field data and centrifuge measurements of excavations in clays and sands indicated that the analytical method is robust for small wall deflection levels (say, for ratios between average wall deflection and wall height β lower than 0.1%), which are frequently achieved in deep wall construction projects. On the other hand, for higher levels of displacements as β greater than 0.3% the model performance was not always satisfactory and often lead to a displacement field wider than field data; this is due to the inelastic ground behaviour close to the wall that is not captured by the analytical method. Also, field and experimental data illustrated that incorporating the ground negative ovalization (when horizontal stress relief is dominant relative to stress relief in the vertical direction) is crucial to obtain satisfactory predictions of the soil movements under most scenarios.
- A summary table was provided to help engineers in their selection of the relative ovalization parameter as a function of ground conditions and wall deflection mode. Back-analyses of real data indicated that parabolic and kick-in deflection modes are associated with similar ovalization ranges for a comparable set of ground conditions, which may differ from the ovalization of composite wall deflections. Thus, the bracing condition of the upper retaining wall has a crucial impact on the ovalization level.

The adopted analytical method relies on the elastic homogeneous isotropic half-space theory. Therefore, this method cannot capture the nonlinear soil behaviour that is expected to occur close to the wall for relatively large wall deflection levels. Future works could refine this analytical solution. This method could benefit from a generalization to layered ground conditions and from the implementation of anisotropic half-space solutions, for which superposition of volume loss solutions is possible, which are not addressed in this paper. Finally, further analytical and numerical insights could be obtained to assess suitable ovalization values, which were empirically related to wall deflection mode and ground conditions in this study.

CRediT authorship contribution statement

Chen Zheng: Conceptualization, Methodology, Software, Formal analysis, Data curation, Writing – original draft. **Andrea Franza:** Conceptualization, Methodology, Writing – review & editing, Visualization, Supervision, Funding acquisition. **Rafael Jimenez:** Conceptualization, Writing – review & editing, Supervision, Funding acquisition.

Declaration of competing interest

The authors declare that they have no known competing financial interests or personal relationships that could have appeared to influence the work reported in the manuscript.

Data availability

Data will be made available on request.

Acknowledgements

This project was partially funded by the European Union's Horizon 2020 Research and Innovation Programme under the Marie Sklodowska-Curie grant agreement No 793715. Partial support was also provided by the Spanish Ministry of Science and Innovation, under Grant PID2019-108060RB-I00. The first author also received financial support provided by the China Scholarship Council (CSC). No. 201706930026.

Appendix A. Supplementary data

Supplementary material related to this article can be found online at https://doi.org/10.1016/j.tust.2023.105316.

References

Boone, S.J., Westland, J., Nusink, R., 1999. Comparative evaluation of building responses to an adjacent braced excavation. Can. Geotech. J. 36 (2), 210–223. http://dx.doi.org/10.1139/t98-100.

Burland, J.B., Hancock, R.J., 1977. Underground car park at the house of commons, London: Geotechnical aspects. Struct. Eng. 55 (2), 81–100.

Cheng, K., Riqing, X., Ying, H.-w., Cungang, L., Gan, X., 2020. Simplified method for calculating ground lateral displacement induced by foundation pit excavation. Eng. Comput. 37 (7), 2501–2516. http://dx.doi.org/10.1108/EC-08-2019-0350.

Cheng, K., Xu, R., Ying, H., Gan, X., Zhang, L., Liu, S., 2021. Observed performance of a 30.2 m deep-large basement excavation in Hangzhou soft clay. Tunn. Undergr. Space Technol. 111, 103872. http://dx.doi.org/10.1016/j.tust.2021.103872.

Clough, G.W., O'Rourke, T.D., 1990. Construction induced movements of insitu walls. In: Proc., Design and Performance of Earth Retaining Structures. Geotechnical Special Publication 25, ASCE, New York, pp. 439–470.

Dan, K., Sahu, R.B., 2018. Estimation of ground movement and wall deflection in braced excavation by minimum potential energy approach. Int. J. Geomech. 18 (7), 04018068. http://dx.doi.org/10.1061/(ASCE)GM.1943-5622.0001105.

Dong, Y.P., Burd, H.J., Houlsby, G.T., 2016. Finite-element analysis of a deep excavation case history. Géotechnique 66 (1), 1–15. http://dx.doi.org/10.1680/jgeot.14.P.234.

Elshafie, M.Z.E.B., Choy, C.K.C., Mair, R.J., 2013. Centrifuge modeling of deep excavations and their interaction with adjacent buildings. Geotech. Test. J. 36 (5), 637–648. http://dx.doi.org/10.1520/GTJ20120209.

Finno, R.J., Atmatzidis, D.K., Perkins, S.B., 1989. Observed performance of a deep excavation in clay. J. Geotech. Eng. 115 (8), 1045–1064. http://dx.doi.org/10.1061/(ASCE)0733-9410(1989)115:8(1045).

Finno, R.J., Calvello, M., 2005. Supported excavations: Observational method and inverse modeling. J. Geotech. Geoenviron. Eng. 131 (7), 826–836. http://dx.doi.org/10.1061/(ASCE)1090-0241(2005)131:7(826).

Finno, R.J., Harahap, I.S., 1991. Finite element analyses of HDR-4 excavation. J. Geotech. Eng. 117 (10), 1590–1609. http://dx.doi.org/10.1061/(ASCE)0733-9410(1991)117:10(1590).

Franza, A., Marshall, A.M., Jimenez, R., 2021. Non-linear soil-pile interaction induced by ground settlements: pile displacements and internal forces. Géotechnique 71 (3), 239–249. http://dx.doi.org/10.1680/jgeot.19.P.078.

Franza, A., Marshall, A.M., Zhou, B., 2019. Greenfield tunnelling in sands: the effects of soil density and relative depth. Géotechnique 69 (4), 297–307. http://dx.doi.org/10.1680/jgeot.17.P.091.

Gaba, A., Hardy, S., Doughty, L., Powrie, W., Selemetas, D., 2017. Guidance on Embedded Retaining Wall Design. Report CIRIA C760, CIRIA, London, UK.

Gaba, A.R., Simpson, B., Beadman, D.R., Powrie, W., 2003. Embedded Retaining Walls: Guidance for Economic Design. Report CIRIA C580, CIRIA, London, UK.

Goldberg, D.T., Jaworski, W.E., Gordon, D., 1976. Lateral Support Systems And Underpinning. Volume II. Design Fundamentals. Report No. FHWA-RD-75-129, United States. Federal Highway Administration, Offices of Research and Development.

González, C., Sagaseta, C., 2001. Patterns of soil deformations around tunnels. Application to the extension of Madrid Metro. Comput. Geotech. 28 (6–7), 445–468. http://dx.doi.org/10.1016/S0266-352X(01)00007-6.

Guo, P., Gong, X., Wang, Y., 2019. Displacement and force analyses of braced structure of deep excavation considering unsymmetrical surcharge effect. Comput. Geotech. 113, 103102. http://dx.doi.org/10.1016/j.compgeo.2019.103102.

Hsieh, P.-G., Ou, C.-Y., 1998. Shape of ground surface settlement profiles caused by excavation. Can. Geotech. J. 35 (6), 1004–1017. http://dx.doi.org/10.1139/t98-056.

Hsiung, B.-C.B., 2020. Observations of the ground and structural behaviours induced by a deep excavation in loose sands. Acta Geotech. 15 (6), 1577–1593. http://dx.doi.org/10.1007/s11440-019-00864-0.

Khoiri, M., Ou, C.Y., 2013. Evaluation of deformation parameter for deep excavation in sand through case histories. Comput. Geotech. 47, 57–67. http://dx.doi.org/10.1016/j.compgeo.2012.06.009.

Kim, S., Finno, R.J., 2019. Inverse analysis of a supported excavation in Chicago. J. Geotech. Geoenviron. Eng. 145 (9), 04019050. http://dx.doi.org/10.1061/(ASCE)GT.1943-5606.0002120.

Korff, M., Mair, R.J., Van Tol, F.A.F., 2016. Pile-soil interaction and settlement effects induced by deep excavations. J. Geotech. Geoenviron. Eng. 142 (8), 04016034. http://dx.doi.org/10.1061/(ASCE)GT.1943-5606.0001434.

Kung, G.T.-C., Hsiao, E.C.-L., Juang, C.H., 2007b. Evaluation of a simplified small-strain soil model for analysis of excavation-induced movements. Can. Geotech. J. 44 (6), 726–736. http://dx.doi.org/10.1139/t07-014.

Kung, G.T., Juang, C.H., Hsiao, E.C., Hashash, Y.M., 2007a. Simplified model for wall deflection and ground-surface settlement caused by braced excavation in clays. J. Geotech. Geoenviron. Eng. 133 (6), 731–747. http://dx.doi.org/10.1061/(ASCE)1090-0241(2007)133:6(731).

Kung, G.T.C., Ou, C.Y., Juang, C.H., 2009. Modeling small-strain behavior of taipei clays for finite element analysis of braced excavations. Comput. Geotech. 36 (1–2), 304–319. http://dx.doi.org/10.1016/j.compgeo.2008.01.007.

Lam, S.Y., Bolton, M.D., 2011. Energy conservation as a principle underlying mobilizable strength design for deep excavations. J. Geotech. Geoenviron. Eng. 137 (11), 1062–1074. http://dx.doi.org/10.1061/(ASCE)GT.1943-5606.0000510.

Lam, S.Y., Haigh, S.K., Bolton, M.D., 2014. Understanding ground deformation mechanisms for multi-propped excavation in soft clay. Soils Found. 54 (3), 296–312. http://dx.doi.org/10.1016/j.sandf.2014.04.005.

Leung, E.H., Ng, C.W., 2007. Wall and ground movements associated with deep excavations supported by cast in situ wall in mixed ground conditions. J. Geotech. Geoenviron. Eng. 133 (2), 129–143. http://dx.doi.org/10.1061/(ASCE)1090-0241(2007)133:2(129).

Liu, G.B., Ng, C.W., Wang, Z.W., 2005. Observed performance of a deep multistrutted excavation in Shanghai soft clays. J. Geotech. Geoenviron. Eng. 131 (8), 1004–1013. http://dx.doi.org/10.1061/(ASCE)1090-0241(2005)131:8(1004).

Liu, Y., Xiang, B., Fu, M., 2019. Observed performance of a large-scale deep triangular excavation in Shanghai soft clays. Geotech. Geol. Eng. 37 (4), 2791–2809. http://dx.doi.org/10.1007/s10706-018-00795-9.

Loganathan, N., Poulos, H.G., 1998. Analytical prediction for tunneling-induced ground movements in clays. J. Geotech. Geoenviron. Eng. 124 (9), 846–856. http://dx.doi.org/10.1061/(ASCE)1090-0241(1998)124:9(846).

Mair, R., 2013. Tunnelling and deep excavations: Ground movements and their effects. In: Proceedings of the 15th European Conference on Soil Mechanics and Geotechnical Engineering–Geotechnics of Hard Soils–Weak Rocks (Part 4). IOS Press, Athens, Greece. pp. 39–70.

Miyoshi, M., 1977. Mechanical behavior of temporary braced wall. In: Proceedings of the 9th International Conference on Soil Mechanics and Foundation Engineering, Tokyo. 2, pp. 655–658.

Mu, L., Huang, M., 2016. Small strain based method for predicting three-dimensional soil displacements induced by braced excavation. Tunn. Undergr. Space Technol. 52, 12–22. http://dx.doi.org/10.1016/j.tust.2015.11.001.

Ng, C.W.W., 1998. Observed performance of multipropped excavation in stiff clay. J. Geotech. Geoenviron. Eng. 124 (9), 889–905. http://dx.doi.org/10.1061/(ASCE)1090-0241(1998)124:9(889).

Ng, C., Hong, Y., Liu, G., Liu, T., 2012. Ground deformations and soil–structure interaction of a multi-propped excavation in Shanghai soft clays. Géotechnique 62 (10), 907–921. http://dx.doi.org/10.1680/geot.10.P.072.

Ng, C.W.W., Wei, J., Poulos, H., Liu, H., 2017. Effects of multipropped excavation on an adjacent floating pile. J. Geotech. Geoenviron. Eng. 143 (7), 04017021. http://dx.doi.org/10.1061/(ASCE)GT.1943-5606.0001696.

Ong, D.E., Leung, C.E., Chow, Y.K., 2006. Pile behavior due to excavation-induced soil movement in clay. I: Stable wall. J. Geotech. Geoenviron. Eng. 132 (1), 36–44. http://dx.doi.org/10.1061/(ASCE)1090-0241(2006)132:1(36).

Osman, A.S., Bolton, M.D., 2004. A new design method for retaining walls in clay. Can. Geotech. J. 41 (3), 451–466. http://dx.doi.org/10.1139/T04-003.

Osman, A.S., Bolton, M.D., 2006. Ground movement predictions for braced excavations in undrained clay. J. Geotech. Geoenviron. Eng. 132 (4), 465–477. http://dx.doi.org/10.1061/(ASCE)1090-0241(2006)132:4(465).

Ou, C.-Y., Hsieh, P.-G., 2011. A simplified method for predicting ground settlement profiles induced by excavation in soft clay. Comput. Geotech. 38 (8), 987–997. http://dx.doi.org/10.1016/j.compgeo.2011.06.008.

Ou, C.-Y., Hsieh, P.-G., Chiou, D.-C., 1993. Characteristics of ground surface settlement during excavation. Can. Geotech. J. 30 (5), 758–767. http://dx.doi.org/10.1139/t93-068.

Ou, C.-Y., Liao, J.-T., Lin, H.-D., 1998. Performance of diaphragm wall constructed using top-down method. J. Geotech. Geoenviron. Eng. 124 (9), 798–808. http://dx.doi.org/10.1061/(ASCE)1090-0241(1998)124:9(798).

Peck, R.B., 1969. Deep excavations and tunneling in soft ground. In: Proc. 7th ICSMFE, Mexico City, International Society for Soil Mechanics and Foundation Engineering. pp. 225–290.

Sagaseta, C., 1987. Analysis of undraind soil deformation due to ground loss. Géotechnique 37 (3), 301–320. http://dx.doi.org/10.1680/geot.1987.37.3.301.

Son, M., Cording, E.J., 2007. Evaluation of building stiffness for building response analysis to excavation-induced ground movements. J. Geotech. Geoenviron. Eng. 133 (8), 995–1002. http://dx.doi.org/10.1061/(ASCE)1090-0241(2007)133:8(995).

Soomro, M.A., Mangnejo, D.A., Bhanbhro, R., Memon, N.A., Memon, M.A., 2019. 3D finite element analysis of pile responses to adjacent excavation in soft clay: Effects of different excavation depths systems relative to a floating pile. Tunn. Undergr. Space Technol. 86, 138–155. http://dx.doi.org/10.1016/j.tust.2019.01.012.

Tan, Y., Wei, B., 2012. Observed behaviors of a long and deep excavation constructed by cut-and-cover technique in Shanghai soft clay. J. Geotech. Geoenviron. Eng. 138 (1), 69–88. http://dx.doi.org/10.1061/(ASCE)GT.1943-5606.0000553.

Verruijt, A., Booker, J.R., 1996. Surface settlements due to deformation of a tunnel in an elastic half plane. Géotechnique 46 (4), 753–756. http://dx.doi.org/10.1680/geot.1996.46.4.753.

Verruijt, A., Booker, J.R., 1998. Discussion: Surface settlements due to deformation of a tunnel in an elastic half plane. Géotechnique 48 (5), 709–713. http://dx.doi.org/10.1680/geot.1998.48.5.709.

Wang, J.H., Xu, Z.H., Wang, W.D., 2010. Wall and ground movements due to deep excavations in Shanghai soft soils. J. Geotech. Geoenviron. Eng. 136 (7), 985–994. http://dx.doi.org/10.1061/(ASCE)GT.1943-5606.0000299.

Xu, K.J., Poulos, H.G., 2000. Theoretical study of pile behaviour induced by a soil cut. In: ISRM International Symposium 2000. International Society for Rock Mechanics and Rock Engineering, Melbourne.

Yoo, C., Lee, D., 2008. Deep excavation-induced ground surface movement characteristics - A numerical investigation. Comput. Geotech. 35 (2), 231–252. http://dx.doi.org/10.1016/j.compgeo.2007.05.002.

Zhang, R., Zheng, J., Pu, H., Zhang, L., 2011. Analysis of excavation-induced responses of loaded pile foundations considering unloading effect. Tunn. Undergr. Space Technol. 26 (2), 320–335. http://dx.doi.org/10.1016/j.tust.2010.11.003.

Zheng, G., Yang, X., Zhou, H., Du, Y., Sun, J., Yu, X., 2018. A simplified prediction method for evaluating tunnel displacement induced by laterally adjacent excavations. Comput. Geotech. 95, 119–128. http://dx.doi.org/10.1016/j.compgeo.2017.10.006.